Chapter 7

Future of n-type PV

Amran Al-Ashouri¹, Mathieu Boccard², Can Han³, Olindo Isabella³, Eike Köhnen¹, Lars Korte¹, Paul Procel³ and Guangtao Yang³

7.1 Introduction

As already discussed in the first chapter of this book, the ultimate efficiency limits of today's PV workhorse, the passivated emitter and rear cell (PERC) technology, are in sight. At the same time, the rate of global solar deployment continues to increase significantly for many leading markets—171 GW_p of PV have been installed globally in 2021, and projections see 209 GW_p to be installed in 2022 and 231 GW_p in 2023 [1]. These two elements create ample opportunity for technologies with higher efficiency potential to increase their market share. Overarching topics in these "beyond PERC" technologies are:

1. Alternative "passivating contacts" technologies. The most prominent of these are the tunnel oxide passivated contact (TOPCon)/polycrystalline silicon on oxide (POLO) and the silicon heterojunction (SHJ) technology, which already today are in the market—and SHJ has been there for quite a while, with the first Sanyo HIT modules being deployed in the late 1990s. In TOPCon/POLO, a thin silicon oxide is used as a passivating interlayer between the c-Si wafer and the highly doped polycrystalline silicon contact layers (cf. also Chapter 3). In SHJ, a few nm of undoped hydrogenated amorphous silicon, a-Si:H, takes the role of the passivating layer, and doped a-Si:H thin films form the carrier selective contacts. Both TOPCon/POLO and SHJ have already demonstrated efficiencies above 26%. Going beyond these technologies, alternative materials, or stacks thereof, are investigated in order to mitigate the few remaining losses, e.g. to achieve higher transparency of the top contacts in the blue/UV

¹Department Perovskite Tandem Solar Cells, Helmholtz-Zentrum Berlin für Materialien und Energie GmbH (HZB), Germany

²Institute of Microengineering (IMT), Photovoltaics and Thin-Film Electronics Laboratory (PV-Lab), Ecole Polytechnique Federale de Lausanne (EPFL), Switzerland

³Photovoltaic Materials and Devices Group, Electrical Sustainable Energy Department, Delft University of Technology, The Netherlands

- and near IR spectral range, or aiming at potentially more cost-effective production processes such as sputtering instead of plasma-enhanced chemical vapor deposition (PECVD), or even wet-chemical in lieu of vacuum processing.
- 2. Tandem and multijunction cells. Even with further improvements in contact layer transparency etc., the practical limit of solar cells based on a single c-Si absorber are in sight, cf. Section 7.3. In order to surpass this limit, multijunction cells can be used, as already demonstrated over the last decades in applications with a different cost structure such as concentrator PV and space applications. For the utility and rooftop market at the TW scale, a different technology will be required, and it can be expected that it will be silicon-based. In Section 7.5, we discuss options for Si-based tandems.

In most of these technologies, n-type wafers have been used to demonstrate highest efficiencies. The reasons for this are summarized in Chapters 2 and 3 on materials and cell concepts; briefly, the benefit of n-type wafers is rooted in the basic physics of point defects in silicon: Most transition metal point defects, as well as silicon surface states have larger electron- than hole capture cross-sections. Therefore, for the same type and concentration of impurities in the crystal, the minority carrier lifetime, i.e. the lifetime of holes in n-type c-Si, is higher than the lifetime of electrons in p-type wafers. This yields a higher potential in both, $V_{\rm oc}$ and fill factor of solar cells on (n)c-Si. Furthermore, conventional boron-doped (p)c-Si is prone to light-induced degradation (LID) through boron—oxygen and/or boron—iron complex formation [2]. This degradation mechanism is not present in (n)c-Si, which makes even relatively oxygen-rich Czochralski wafers a viable option for the high efficiency cells discussed in the following.

7.2 Carrier-selective passivated contacts

As we will see in the following sections, all of today's as well as, most likely, future very high efficiency silicon solar cells are based on so-called carrier selective passivated contacts (CSPCs). What are the differences of such CSPCs to the diffused junctions used traditionally in photovoltaics?

In very general terms, a solar cell under illumination can be understood as a device where electrons and holes are generated by the impinging photons in an absorber (in our case, the silicon wafer), and these charges are then extracted selectively through two contacts according to their polarity, cf. Figure 7.1(a). Such selectivity for just one carrier type is achieved through asymmetric conductivities for the two carrier types. In Figure 7.1(b), this idea is depicted for an electron-selective contact: It has a high conductivity for electrons, σ_e , much greater than the conductivity for holes, σ_h . Therefore, a large current of electrons toward the contact can be sustained with just a small driving force, i.e. a small gradient of the quasi-Fermi level of electrons (dashed blue line). However, with a small σ_h , the hole current to this contact will also be small even with a large gradient of the quasi-Fermi level of holes (dashed red line). In traditional diffused junction cells, this selectivity, i.e. large difference of conductivities, is achieved through doping, cf. Figure 7.1(c). This works

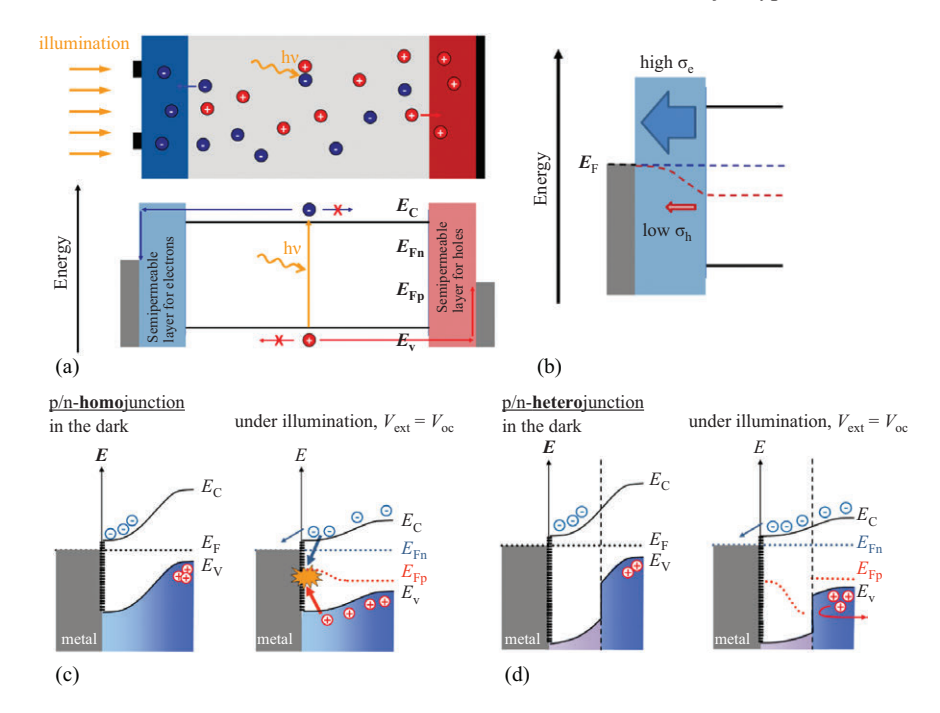


Figure 7.1 (a) Schematic of a generic solar cell structure with semipermeable layers which selectively extract photogenerated electrons (left) and holes (right) to the contacts. Bottom: simplified band diagram. (b) Generic band diagram of a semipermeable layer with high conductivity σ_e for electrons, but low conductivity σ_h for holes. (c) Band diagram of an n/p junction, and (d) of an electron-selective heterojunction in the dark and under illumination. Black dashes at the metal/semiconductor interface represent interfacial defects

reasonably well in the dark, where a high density of electrons close to the contact ensures high electron conductivity, whereas the hole density is low, yielding a low conductivity for holes.* However, under illumination, the density of both electrons and holes is greatly enhanced, in high injection conditions even surpassing the doping-induced density of majority carriers in the bulk of the wafer (holes, for the case of p-type c-Si sketched here). The conductivity is the product of charge carrier mobility, μ_i , and concentration, n_i : $\sigma_i = \pm q \, n_i \, \mu_i$, where the index i represents electrons (e) or holes (h) and q is the elementary charge. Thus, when the densities of

^{*}This discussion is inspired by the work of Würfel *et al.* [3], and it is different from the usual textbook arguments involving electrical fields in the p/n junction, which are said to repel and attract opposite charge types. In the framework of this theory, the electrical fields in such junctions are merely a byproduct of the different carrier densities, thus conductivities, achieved by doping. See e.g. Ref. [4] for further implications of this approach to understanding carrier selectivity.

electrons and holes become similar under illumination, conductivities towards the contacts also become similar in diffused junctions since the mobilities $\mu_{\rm p}$ and $\mu_{\rm n}$ in silicon differ by less than half an order of magnitude. Therefore, Shockley-Read-Hall (SRH) recombination across defects at the semiconductor/metal interface will become very efficient, since both electrons and holes are then present at the interface in large quantities. This strong recombination limits the quasi-Fermi level splitting in the wafer bulk, thus the V_{oc} of the solar cell. However, if the diffused junction is replaced by a heterostructure, i.e. a second semiconductor deposited on the c-Si wafer that gives rise to an asymmetric band offset, this problem can be resolved, cf. Figure 7.1(d): As sketched here, the holes see a large barrier that they cannot overcome even when the bands are flattened out under illumination. Thus, the concentration of holes at the recombination active interface is greatly reduced, and so is the SRH recombination. This is why such contacts, where the recombination-active interface is separated from the absorber by a semipermeable layer, are called "passivated". On the other hand, electrons are not hindered (in this ideal case) by an additional barrier and thus can move freely to the contact to be extracted. This is the difference between passivated surfaces/interfaces (such as c-Si/SiO₂, c-Si/AlO_x, etc.[†]) and carrierselective passivated contacts (CSPCs): the latter still allow to extract one charge carrier type, while the former block both carrier types.

In the following sections, we will see how this general concept of CSPCs is implemented both in already industrialized as well as in future high efficiency cell concepts. In practical devices, the passivating CSCs often consist of double-layer stacks, where the layer adjacent to the wafer serves to passivate the c-Si surface and a second, highly doped and thus highly conductive layer improves carrier selectivity. In addition, a third layer—often a transparent conductive oxide (TCO)—may be required to provide sufficient lateral conductivity to the contact fingers.

7.2.1 Silicon heterojunction solar cells

Silicon heterojunction (SHJ) solar cells hold the world record of power conversion efficiency (PCE) among single-junction solar cells, with 26.81% and 26.7% as front-back contact and interdigitated back-contact devices, respectively [5–9]. The key feature of SHJ cells is a particularly high open-circuit voltage ($V_{\rm oc}$) due to the excellent passivation provided by hydrogenated amorphous silicon stacks [10] deposited on high-quality monocrystalline wafers. SHJ cells also show a lower temperature coefficient than diffused-junction devices, enhancing their energy yield in the field as compared to classical Si cells [11]. From a manufacturing point of view, the fabrication of HJT solar cells requires only unstructured blanket layer depositions (except the metal contact grid) and a reduced number of process steps compared to their mainstream counterparts, yielding a relatively low CAPEX [11]. Due to the combination of these advantageous features, especially the superior energy yield and

[†]Note that SiO₂, etc. are also used in CSCs, e.g. in TopCon/POLO type junctions. However, for this purpose, they are made ultrathin, of the order of 1 nm, so that charges can cross the barrier by quantum-mechanical tunneling.

simple fabrication process, SHJ solar cells are expected to continuously gain market share in the coming years [12]. For the same reasons, they are also considered an excellent candidate for the bottom cell of Si/perovskite tandem devices [13].

The progression in best SHJ cell efficiencies over the last 30 years is shown in Figure 7.2(b). Many aspects of the SHJ device concept will be discussed only briefly in the following. For further reading, several review articles [11,14–16] and a monograph [17] on the same subject are recommended.

Silicon heterojunction device structure and history: A schematic layer stack and a band diagram for a both sides contacted SHJ cell on n-type wafer and with p/n junction on the front is depicted in Figure 7.2(a). The key feature of SHJ solar cells are stacks of a few nm thin hydrogenated amorphous silicon (a-Si:H) films deposited on the crystalline silicon absorber. They are typically grown by plasmaenhanced chemical vapor deposition (PECVD) at temperatures around 200°C. The hydrogen, which is present in the a-Si:H at a level of a few percent, passivates both internal defects of the amorphous silicon network, and most of the remaining dangling bonds at the a-Si:H/c-Si interface. Device grade a-Si:H has a band gap of the order of 1.7 eV, with asymmetric band offsets to c-Si [18]. As can be seen from the band diagram in Figure 7.2(a), the amorphous/crystalline silicon heterojunction is thus not ideally suited for charge carrier extraction from the crystalline silicon absorber: Instead of providing a high band offset, thus a high barrier, for one carrier type and a vanishing one (no band offset) for the other, both carrier types "see" barriers. Furthermore, these barriers are the same for both the electron and hole contacts. This is why the additional doped layers are required: They define the

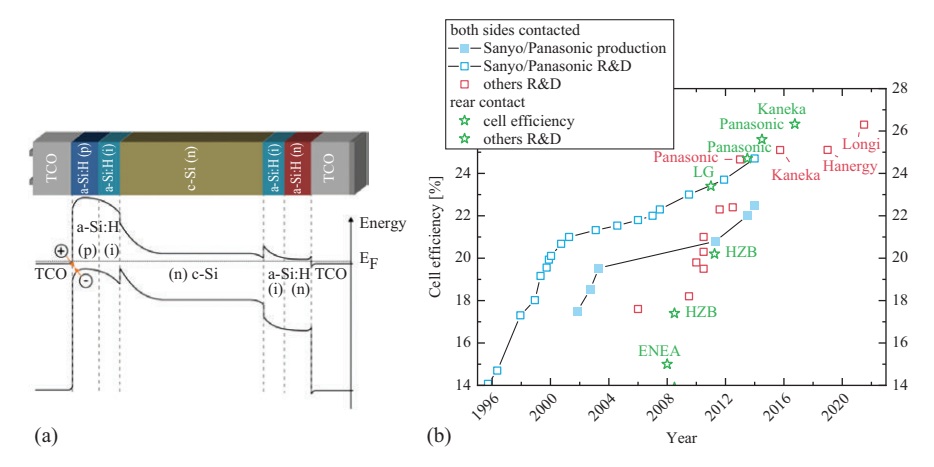


Figure 7.2 (a) Schematic of a front-back contacted silicon heterojunction solar cell with p/n junction on the front side (illuminated from the left side), and the corresponding band diagram. (b) Development of silicon heterojunction cell efficiencies over the last 30 years. All both sides contacted cells reported after the year 2000 are >100 cm², while rear contact devices are small (1 or 4 cm²) as well as large area.

direction of the current flow by providing a high conductivity for the desired carrier polarity. The a-Si:H/c-Si junction will thus function as a passivating CSC which separates the contacts (where the density of electronic defects is high) spatially and electronically from the c-Si absorber. The concept of amorphous/crystalline silicon heterojunctions was introduced by Fuhs et al. in the 1970s using a direct heterojunction between doped a-Si:H and c-Si [19]. In the 1990s, the company Sanyo introduced an additional, undoped, thus nominally intrinsic (i) a-Si:H buffer layer between the doped a-Si:H films and the c-Si wafer [20]. Due to the absence of dopants, the (i) a-Si:H interlayer has much reduced defect densities and can be finetuned to minimize a-Si:/c-Si interface recombination, which enabled SHJ cell $V_{\rm oc}$ s above 700 mV. Further process steps in the fabrication of SHJ cells comprise: (i) the deposition of TCO layers, typically sputter-deposited indium-tin oxide or other indium-based oxides, on top of the a-Si:H. The TCO serves as antireflection coating and at the same time enables lateral carrier transport to the contact grid fingers. (ii) Screen-printing of front and rear side metallizations, using low-temperature curable silver pastes, and (iii) a final curing step for the paste, which serves at the same time to anneal defects present in the a-Si:H either from the initial PECVD or the subsequent TCO sputtering. Overall, the cell process is based on comparatively simple full-area deposition steps and screen-printed contacts. This is in contrast to conventional c-Si cells with diffused emitters where efficiencies well above 20% can only be reached using local contacting schemes requiring additional patterning. Furthermore, since all process steps occur at temperatures around or below 200°C, SHJ cell fabrication has a low thermal budget. In contrast to conventional diffusion processes that lead to wafer bowing and increased breakage, the SHJ process is compatible with very thin wafers: for example, a 24.7% cell with 102 cm² total area was fabricated on a 98 μ m thin wafer [21].

The use of an intrinsic passivating interlayer was patented by Sanyo (and marketed as HIT® technology). Over 20 years, Sanyo, then Panasonic, have produced more than 500MW/a of HIT modules [22], i.e. a cumulated SHJ production of around 10 GW. Inspecting Figure 7.2(b), it is obvious that around 2010, also other institutes and PV manufacturers have started to demonstrate significant improvements in cell efficiency. Interestingly, this steep increase in PCEs coincides with the expiration of the (i) a-Si:H patent.

State of the art: As mentioned above, the highest reported power conversion efficiency for a double-side contacted silicon cell to date was reported in November 2022 by the Chinese PV company LONGi, with a 26.81% SHJ cell on an M6 wafer (cell area 274 cm²) [5,8]. The excellent passivation of c-Si surface defects by the heterojunction also results in the highest reported open circuit voltage ($V_{\rm OC}$) for silicon solar cells of 751 mV, on par with a previously achieved $V_{\rm oc}$ result, also with SHJ, by Panasonic [23]. Instead of doped amorphous silicon layers, at least for the n-type contact, nanocrystalline films are used in this SHJ. This probably also contributes to the efficient carrier extraction demonstrated by the extremely high fill factor of 86.1%, as well as to the high current density $j_{\rm sc}$ of 41.45 mA/cm².

The $j_{\rm sc}$ is the only individual parameter where interdigitated back side contacted (IBC) SHJ can outperform their double-side contacted siblings. Until recently, IBC SHJ cells also held the overall world record for silicon solar cells, with a PCE of 26.7% ($V_{\rm oc}$ 738 mV, $j_{\rm sc}$ 42.65 mA/cm², FF 84.9%; designated measurement area: 79 cm²), realized by Kaneka [6,7]. As also discussed in Ref. [7], the "practical limit" for SHJ-based solar cells is estimated at around 27.1%, probably to be achieved with a back contacted cell due to the further reduced optical absorption losses in this geometry. Thus, the present record results are only a few tenths of a percent from this "practical limit."

Future R&D requirements: According to a market analysis performed at the end of 2020 [24], about 20 companies had expressed interest in starting SHJ manufacturing, and at least four (REC, GS Solar, Tongwei, Hevel) have started production already. Moving forward, the following points are likely to be key to reaching highest efficiencies and cost competitiveness. A more in-depth discussion of some of these points can be found e.g. in the review by Haschke *et al.* [11]. Note that module technology aspects are not considered here.

(i) As discussed e.g. in [15], the availability of silicon wafers with very high carrier lifetime is crucial not only to achieve a high $V_{\rm oc}$, but even more so for realizing ultimate fill factors: If recombination at bulk and interface defects can be suppressed to a level where Auger recombination dominates the carrier lifetime also at the maximum power point, diode ideality factors below 1 become possible. This translates into fill factors approaching the ideal value of \sim 89% (assuming only Auger recombination and no series resistance [15]).

To improve the SHJ cell's optics, thus the $j_{\rm sc}$, a more transparent front side is desired. Several aspects need to be considered, which can also have considerable influence on production costs:

(ii) Light absorbed in the doped amorphous silicon layers does not contribute to the SHJ's photocurrent, since minority carrier lifetimes in these layers are very low. To reduce this parasitic absorption, alternative Si-based doped layers with wider band gaps and/or lower absorption coefficients have been explored, such as amorphous or nanocrystalline silicon carbide, a-/nc-SiC [25,26], or nanocrystalline silicon oxide, nc-SiO_x [27,28].⁴ Furthermore, it was found that p-doped a-Si:H films have inferior optical and electrical properties (lower doping efficiency; higher defect densities, thus parasitic sub-bandgap absorption; smaller band gap) than intrinsic and n-type films. Therefore, it is beneficial to place the (p)a-Si:H (or (p) nc-Si:H) film on the SHJ cell's rear side. On an n-type c-Si wafer, this creates a rear p/n junction cell with inverted polarity as compared to Figure 7.2(a). Note that such devices are often called "rear emitter" cells, but this is actually a misnomer [29].

³Note that a "practical limit" FF of 85.3% was estimated for the 27.1% "practical efficiency limit." Taking the 86.6% of the double-side contacted record SHJ, this would scale to slightly higher "practical efficiency limit" of 27.5%. However, it is unclear whether such a high FF can also be achieved in an interdigitated rear contact geometry, where the contact area has to be shared by both contacts and the series resistance is thus likely to be higher.

⁴Historically, such films were labeled as "microcrystalline," due to the visibility of features on the μ m scale e.g. in SEM images. The actual crystallites have sizes in the nm scale, though.

- (iii) Placing the p/n junction on the cell's rear side has additional benefits for lateral charge transport towards the grid fingers on the front side of the cell: with an n-doped a-Si:H (or nc-SiO:H) film on the front, an electron accumulation layer is formed. This helps in transporting the photogenerated current toward the grid fingers, and the front side TCO can therefore have a higher sheet resistance [30]. This enables to use more oxidic versions of the "standard" TCO, i.e. indium tin oxide (ITO), which show less free carrier absorption (FCA) in the near IR range due to reduced carrier densities, thus improving the near-IR EQE and overall isc. Other Inbased TCOs such as InO:H [31] show improved electrical properties (increased electron mobilities), allowing for low carrier concentration and high IR transparency while maintaining high conductivity. However, all In-based TCOs share the same cost risks: The \sim 80 nm thick ITO films which are typically deposited on the front and back of SHJ cells consume about 3.5 g of Indium/m² of modules, costing $\sim 1 \text{ }^2$, or below 0.5 ct/W for a 335 W, 60 cell module [11]. However, the In price is relatively volatile, it has been fluctuating by a factor of 2 over the last 10 years. To mitigate this cost risk, alternative In-free TCOs such as aluminiumdoped zinc oxide (ZnO:Al) can be attractive, especially for the SHJ cell's front side in combination with the rear p/n junction geometry. Indeed, rear junction SHJ with ZnO:Al and identical performance as the ITO references as well as good stability under damp-heat tests have been demonstrated recently [32,33]; combinations of In-containing and In-free TCOs could also be an attractive option to reduce overall In consumption [34]. The topic of alternative TCOs also has a direct connection to alternative carrier-selective contacts as discussed in Section 7.4.
- (iv) Another cost driver in SHJ cells is the contact metallization: due to the low annealing temperatures of only $\sim\!200^{\circ}\text{C}$ allowed for SHJ due to the presence of the a-Si:H films, low-curing-temperature silver screen printing pastes need to be used. The conductivities of such pastes have been greatly improved over the last 10 years, approaching the specific bulk resistivity of Ag ([11], Figure 7.10). Still, alternative concepts for cell contacting, such as copper plating, reviewed in Ref. [35] or the so-called SmartWire technology [36] are interesting. Ref. [37] presents an overview over these diverse options.
- (vi) Finally, the remaining parasitic light absorption in the front contact formed by the silicon layer stack together with the TCO, as well as the shading by the metal grid can be avoided altogether by using highly transparent passivation layers such as SiO_x/SiN_x on the front and placing both contacts on the rear side of the cell. A geometry of alternating p- and n-type stripe contacts is used in the already mentioned interdigitated back contact silicon heterojunction (IBC-SHJ) cell concept. As discussed above, IBC-SHJ hold the record for the highest solar cell efficiency in a single junction silicon cell to date, of 26.7% [7]. While it appears that such IBC-SHJ cells will probably be the devices to demonstrate ultimate efficiencies also in future, practical issues remain especially in structuring the a-Si:H, TCO and metal films of the IBC, which might also lead a cost penalty [38]. However, notable progress has been made in simplifying these structuring steps by using shadow masks during silicon thin film and TCO deposition, requiring just a single alignment step to define the n and p contact areas [39]. Note, that the IBC geometry with two contacts at the

cell's back also opens up entirely new options also for tandem solar cells, enabling three-terminal tandem configurations [40] with enhanced energy yield also under conditions with pronounced spectral mismatch, cf. Section 7.5.

7.2.2 TOPCon/POLO

History: The theoretical efficiency of the PERC cell, which dominates the current PV market, is limited to 24.5% due to the high metallization induced recombination. To further push the c-Si cell efficiency to its limit, different passivating contact concepts have been introduced, which are able to bring c-Si cell efficiencies closer to their ultimate limit around 29% [41]. Besides the silicon heterojunction and doping free passivating contacts, passivating contacts based on poly-Si on ultra-thin silicon oxide have also proven to enable record high efficiencies, with the so-called tunneling oxide passivating contact (TOPCon) [42] and poly-Si on oxide (POLO) solar cell structures [43]. The poly-Si/silicon oxide concept was first introduced into the PV field with the so-called semi-insulating poly-Si (SIPOS) hetero-contact by Yablonovitch et al., which led to a $V_{\rm OC}$ of 720 mV in a solar cell test structure [44]. The first solar cell device with this contact structure showed a cell efficiency of 12% [45]. Recently, together with the demonstration of record efficiencies of c-Si solar cells with passivating contacts, the SiO_x/poly-Si as one of the most promising contact structures has drawn extensive attention from PV research institutes and industry.

Working principle: The poly-Si-based passivating contact structure consists of a highly doped poly-Si on an ultra-thin silicon oxide (SiO_x) layer, see Figure 7.3(a). The ultra-thin SiO_x layer plays a role as chemical passivation layer for the c-Si surface, but also builds a potential barrier for the carriers' transport through it, see Figure 7.3(b). Owing to a much higher doping level within the poly-Si layer than that in the c-Si bulk, see Figure 7.3(c,d), an electrical field is built up at the c-Si interface, which enables field effect passivation of the c-Si surface and carrier selective collection, see Figure 7.3(a). The doping profile at the interface is a crucial factor that influences the electrical field passivation quality, see the inset tables in Figure 7.3(c,d), as well as the transport of the majority carriers: the optimization of the doping tail inside the c-Si surface region induces an efficient separation of carriers inside the c-Si bulk before they reach the c-Si surface with its high defect density D_{it} . On the other hand, by alloying the poly-Si with oxygen [46–48], carbon [49,50], and nitrogen [51], the modified electronic properties of the formed layer can eventually improve the carrier selective collection.

Passivation/hydrogenation: Besides the chemical passivation induced by the ultra-thin SiO_x and the field effect passivation due to the high doping within the poly-Si layer, hydrogen passivation of the c-Si surface defects is another key factor that contributes to the passivation quality of this passivating contact structure. The hydrogen passivation process is also referred to as hydrogenation, which is achieved by introducing hydrogen atoms to the c-Si surface to saturate the Si dangling bonds. Hydrogenation is normally done by diffusing hydrogen species from a solid [52–54], gas [52], or ionized [55] hydrogen source at a high temperature between 400°C and 850°C. The accumulation of hydrogen atoms at the c-Si/SiO_x/poly-Si interfaces [53] minimizes the c-Si surface defect density,

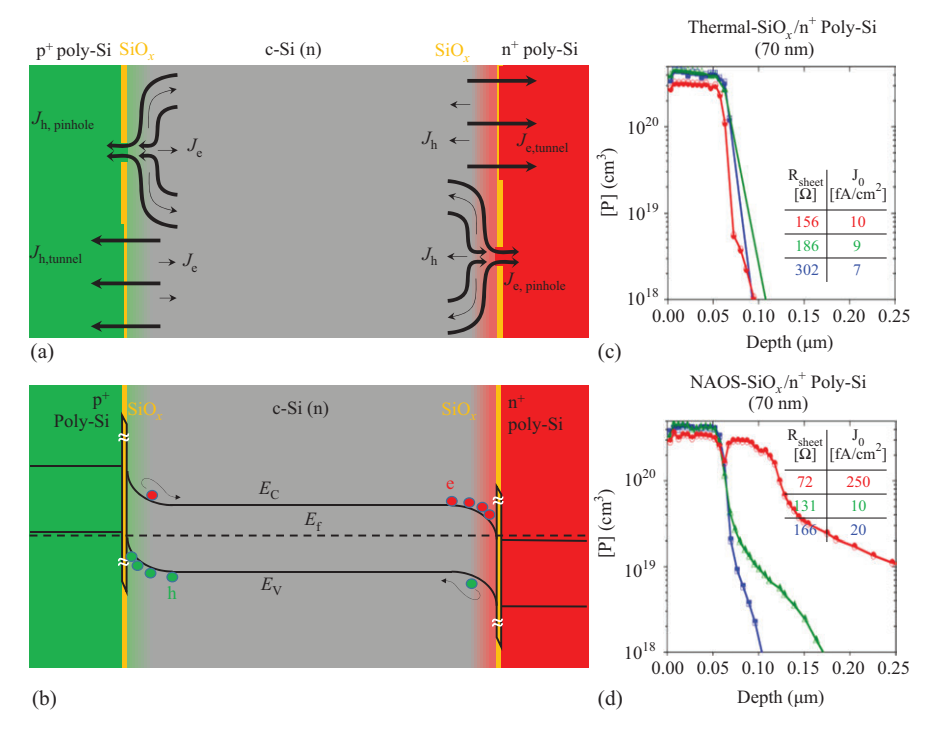


Figure 7.3 (a) Schematic sketch of poly-Si passivating contact and charge transport into n⁺ and p⁺ poly-Si based on tunneling and pinholes structure. (b) Band diagram of the n⁺ and p⁺ poly-Si passivated contacts on n-type c-Si wafer. The doping profiles of phosphorous, P, in n⁺ poly-Si passivating contacts prepared with (c) thermal-SiO_x and (d) NAOS-SiO_x as interfacial layer. Replot based on Ref. [56]

therefore reducing the c-Si surface recombination velocity. The quality of passivation is quantified by the recombination current density J_0 . The lower the J_0 value the better the passivation.

Carrier collection: The type of carrier extracted at the contact is determined by the doping type of the poly-Si layer. The carrier selectivity for holes and electrons, $S_{10,h}$ and $S_{10,e}$ respectively, has been discussed in the literature [57]. They influence the recombination parameter J_0 and the difficulty of carrier transport through the contact stack, quantified by the contact resistivity $\rho_{\rm C}$. This means that the carrier selectivity optimization of the poly-Si passivating contact stands for the minimization of the aforementioned J_0 at the c-Si surface, together with minimization of $\rho_{\rm C}$. For $\rho_{\rm C}$, besides influences from the doping level and doping profile of the contact structure, the quality and thickness of the thin-SiO_x layer are also dominating factors. Especially the SiO_x layer thickness is a crucial parameter that determines the carrier transport mechanisms, by tunneling (for SiO_x thickness < 1.5 nm) or through pinholes

(for thicker SiO_x layers), see Figure 7.3(a). The pinholes within in the thick SiO_x layers are usually formed by high-temperature annealing processes during the activation/diffusion of the dopants within the poly-Si layer, which also leads to locally thinned SiO_x regions [58,59].

Preparation technology: The fabrication of the poly-Si-based passivation contacts mainly consists in the following five steps: [1] formation of the ultra-thin SiO_x layer, [2] poly-Si layer deposition, [3] doping process, [4] high-temperature annealing and [5] hydrogenation process. Different process technologies were explored to study the influences of material properties on the performance of the contact structures. For example, the ultra-thin SiO_x layer has been prepared by thermal-oxidation [60], oxygen-plasma oxide [51], chemical-oxidation with nitric acid [61], sulfuric acid [62], hydrogen peroxide [63], ozone-based oxides [64], and ALD prepared SiO_x [65]. The poly-Si layers can be deposited by PECVD [66], LPCVD [67], and PVD [68]. In practice, depending on the used technologies for each step, a few of the aforementioned steps can be integrated into one single step. For example, it is possible to integrate the first two or even three steps into one single process step by using a thermal/plasma-SiO_x layer, which is followed by intrinsic/in-situ doped a-Si layer deposition with LPCVD or PVD technology [51,69–71].

Solar cell structure and efficiency evolution: The application of poly-Si-based passivating contacts in c-Si solar cells can be grouped into front/back contact (FBC) solar cells and interdigitated back-contact (IBC) solar cells. A FBC cell can feature one poly-Si contact, for example, the TOPCon [72] and iTOPCon [71] cell, or two poly-Si contacts with localized poly-Si contact regions [73] or on the full surface area [74]. An IBC solar cell can also feature one or two contacts with poly-Si/SiO_x/c-Si junctions. The cell sketches are shown in Figure 7.4 (left).

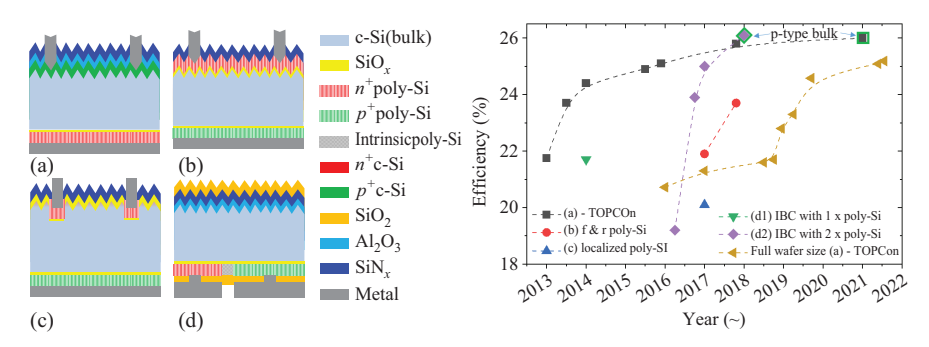


Figure 7.4 Left: Sketch examples of solar cells that deploy poly-Si CSPC structure. (a) One polarization TOPCon cell, (b) two polarizations on full area poly-poly FBC, (c) localized poly-Si contact poly-finger FBC cell, and (d) interdigitated back contacted solar cells poly-Si IBC. Re-sketch based on reference [16]. Right: The efficiency evolution of n-type solar cells with different structures, shown on the left, fabricated with poly-Si-based passivating contacts. Data taken from Refs. [42,49,56,60,61,71–73,75–87]

The efficiency of n-type solar cells with one or two poly-Si contacts progresses rapidly, for both laboratory scale and commercial scale cells, along with the optimization of the poly-Si passivating contact and a deeper understanding of the physics background. In Figure 7.4 (right), we present the efficiency evolution of n-type solar cells with different structures fabricated with poly-Si-based passivating contacts, from < 20% laboratory scale efficiency in 2013 to >25% full wafer size commercial scale cell efficiency in 2021. Note that by 2022 the highest TOPCon cell efficiency is 26.4% as announced by Jinko with a n-type large area solar cell [193].

7.2.3 Bifacial cells

7.2.3.1 Bifacial solar cell development

The idea behind bifacial solar cell designs is to make them light sensitive on both sides of the substrate, such that the absorption of sunlight can be maximized and the energy yield can ultimately be improved. The history of bifacial cell concepts starts as early as 1960 [88]. However, it was only around 1980 that scientists realized that a bifacial solar cell could also be sensitive to the natural albedo [89], i.e., reflected and scattered light from the surroundings [90]. Since the 1990s, the University of New South Wales (UNSW) has been developing bifacial metallization alternatives to achieve high efficiency bifacial solar cells [91-93]. Figure 7.5 summarizes the efficiency evolution of c-Si based bifacial solar cells as reported in literature. Besides, there are newly developed concepts such as thin-film or tandem-based bifacial solar cells [94-101], which are beyond the scope of this book. From Figure 7.5, one can see that (i) with respect to p-type cell technologies, n-type cells are gaining more momentum. This could be attributed to their higher efficiency potential, little LID and less sensitivity to degradation upon high-temperature processing [102]. (ii) Regarding the bifacial cell structure evolution, bifacial buried contact solar cells (BCSCs) were proposed and developed by UNSW in the 1990s [91,103]. However, such BCSCs suffered from high recombination losses, and the controllability in processing the grooves and in the metallization steps was not sufficient [104]. In the past decade, BCSC [105] was replaced by PERx technologies such as PERC (passivated emitter and rear contact), PERT (passivated emitter, rear totally diffused), and PERL (passivated emitter, rear locally diffused). Furthermore, bifacial c-Si solar cells with carrier selective passivating contacts (CSPCs) are becoming more attractive due to the high efficiency potential, such as silicon heterojunction (SHJ), and Tunnel Oxide Passivated Contact (TOPCon). So far, the highest bifacial cell efficiency is 25.4% as reported by Jinko with an n-TOPCon solar cell structure [105].

7.2.3.2 Bifacial solar cells in the PV market

Figure 7.6(a) displays the status of bifacial cells in the PV market. PERC is currently dominating the market, due to its relatively high cell efficiency and low production cost. It is noteworthy that the cost of bifacial PERC cells has been close to that of monofacial cells [89]. Moreover, one should take into consideration the energy yield gain due to bifacial cell use [121]. The bifaciality factor (which is the

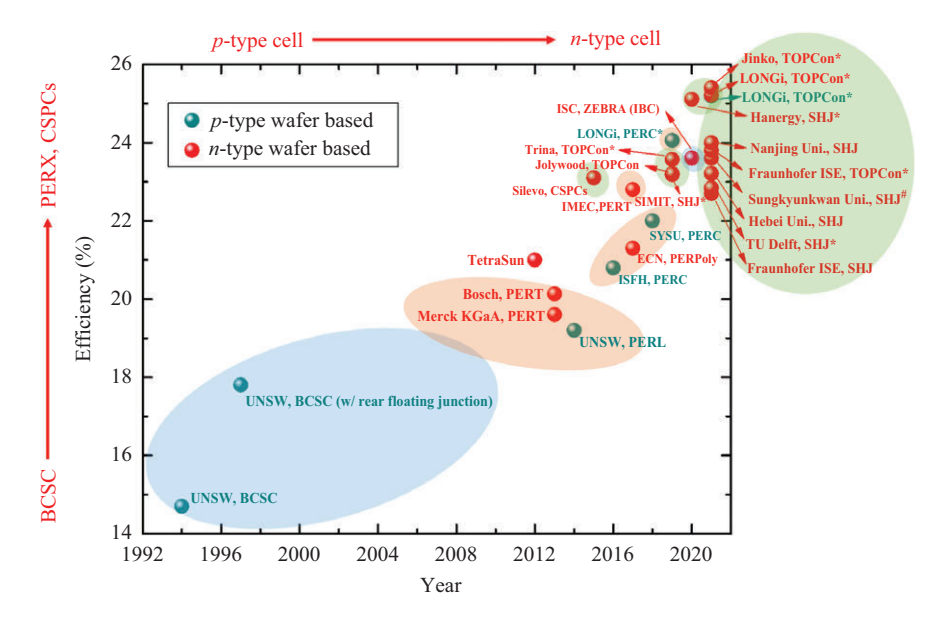


Figure 7.5 The efficiency evolution of c-Si-based bifacial solar cells as reported in literature [71,87,91,92,106–120], in which the bluish background indicates the buried contact solar cells (BCSCs); the yellowish background denotes the PERX cells, and the greenish background depicts c-Si solar cells with carrier selective passivating contacts (CSPCs). Note: unless indicated with with a "#," the cell performance was measured with single-side illumination; The "*" implies that the data was certified from a third party institution

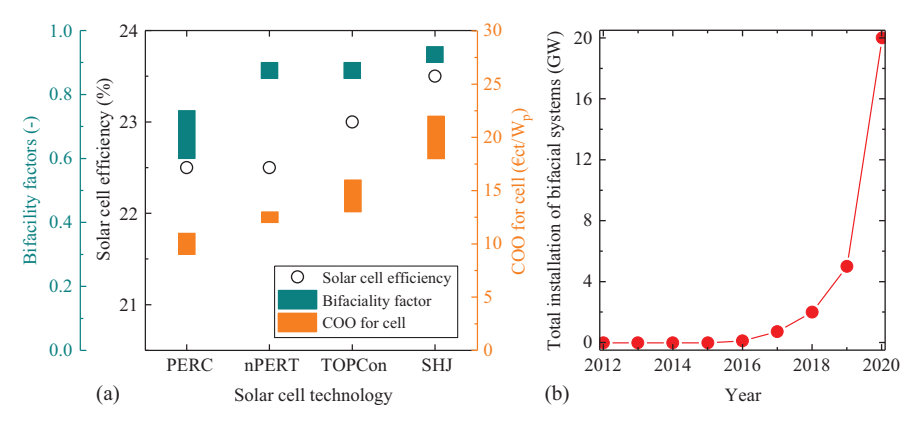


Figure 7.6 (a) Bifacial solar cell efficiency, bifaciality factor, and cost of ownership (COO) as a function of solar cell technologies and (b) accumulated capacity of bifacial PV systems. The data were obtained from [102]

ratio of the one-side efficiency to the efficiency under illumination from the other side under standard test conditions) of PERC cell is in the range of 0.60–0.75. For comparison, c-Si cells with CSPCs (such as TOPCon and SHJ) show both higher efficiency and bifacility factors, but the costs of such cells are also higher. Figure 7.6(b) depicts the accumulated capacity of bifacial PV systems. Historically, the world's first bifacial PV module was launched in 2000 by Sanyo (now Panasonic), based on its proprietary heterojunction with intrinsic thin layer (HIT) design [122]. However, it was only after 2010 that the first >1 MW_p system was built in Japan by a private investor with bifacial nPERT modules [102]. In the following 10 years, with more and more players involved (such as MegaCell, Sunpreme, Yingli, SolarWorld, LONGi, Jolywood) [102,123], bifacial modules became more readily available. In particular, bifacial PV is becoming bankable [89,102] and is expected to play an important role in future electricity generation.

7.2.3.3 Prospects and challenges of bifacial PV

After decades of development, bifacial cells are now able to deliver high efficiencies above 25% (single-side illumination), bifacial modules have become available on the market, and bifacial PV is becoming bankable. Besides, an International Electrotechnical Commission (IEC) specification to measure and label bifacial PV products is available since 2019 [124]. This represents an important step forward toward standardization. Furthermore, different energy yield simulation tools have been developed which could take bifaciality into account [90]. However, when more detailed and precise simulations are required, more advanced programs remain to be developed and deployed [102]. On the other hand, next-generation PV technology remains to be considered. As PERC is coming to its efficiency limit, novel cell concepts need to be implemented in production lines. Both TOPCon and SHJ are promising technologies. TOPCon could be easily integrated from upgrading existing PERC lines, while SHJ implementation may face higher Capex (capital expenditure) due to equipment incompatibility. However, comprehensive long-term cost analyses still need to be performed. Furthermore, the following items still need to be addressed: (i) continuous improvements of different bifacial PV technologies, including c-Si based, thin film or tandem-based; (ii) integration of bifacial PV into various applications, such as utility-scale PV, agrivoltaics, BIPV; (iii) advanced metallization and interconnection designs, in order to maximize power output with minimal use of expensive materials; and (iv) other innovations at module/system level, such as material choice of transparent cover, tracker/tilt design in bifacial module installation.

7.3 Ultimate efficiency in c-Si PV

Silicon is an element (material) that is abundant in earth and features a bandgap of 1.1 eV, close to the optimal bandgap for AM1.5 spectrum for PV applications according to the Shockley–Queisser (SQ) limit for a single junction. However, owing to the indirect band gap of Si, silicon solar cells are not able to reach this limit. The indirect

bandgap reduces the probability for both absorption and radiative recombination, resulting in a relatively weak absorption and the dominance of Auger recombination, respectively. Considering such drawbacks, the limiting efficiency has been calculated to 29.43% for $110 \, \mu \text{m}$ thick un-doped silicon [125].

To overcome the low absorption, thicker silicon wafers are required. In addition, c-Si solar cells demand advanced light management techniques to trap most of the light inside the absorber. Thus, these light trapping methods are focused on reducing optical losses by, for instance, using nano-texturing [126] or multi-anti-reflective coatings (ARC) in the front side together with distributed Bragg reflectors [127] on the rear side. However, the implementation of such upgrades in c-Si solar cells implies modifications at interfaces and thus might entail new technological challenges for mitigating recombination and improving the transport of carriers toward electrodes.

In general, recombination mechanisms limit the conversion efficiency. Important improvements have been reported in mitigating SRH recombination due to defects at interfaces and also inside the absorber bulk. In principle, metallic electrodes were in direct contact to the absorber bulk yielding highly defective c-Si/metal interfaces with strong recombination. The development and implementation of the so-called passivating contacts allowed to overcome the limitation of recombination at interfaces. Similarly, important technology improvements have been developed to mitigate defects in the bulk and thus reducing recombination [128,129]. Indeed, such high lifetime materials expose the interesting behavior of intrinsic recombination in c-Si. Thus, relevant calibration of the semi-empirical models of intrinsic recombination have been reported lately [130–134]. Interestingly, the theoretical limiting efficiency calculated with updated Auger parameterizations exhibits slight variations in the range of 29.4–29.6% [134].

It is well known that Auger recombination increases with the doping, suggesting that minimal recombination is achieved for un-doped silicon. However, intrinsic recombination also depends on the injection of free carriers, that becomes relevant for relatively low doping. Indeed, considering the AM 1.5 spectrum and maximum power conditions, a slight increase of intrinsic recombination is calculated until 10^{15} cm⁻³ doping as reported by Richter *et al.* [125] (see Figure 7.7). For higher doping above 10^{15} cm⁻³ the intrinsic recombination significantly increases (see red arrow in figure), while a slight decrease is calculated for lower doping (see green arrow in Figure 7.7). This means that the practical limiting efficiency could be enabled for solar cells using wafers with resistivity above $10~\Omega^*$ cm with high quality (lifetime) and using passivating contacts.

The limiting efficiency was calculated for around $100 \, \mu m$ thick silicon wafer [125] (Figure 7.8). Such a value is result of the optimal trade-off between absorbed light and intrinsic recombination in a 1D device model [125,134]. Note that both mechanisms increase with the thickness. In fact, intrinsic recombination increases with the thickness due to the increment of the path for collecting carriers that becomes optimal in the simplified 1D picture. However, in real solar cells, the collecting path becomes 2D and even 3D depending on the design and architecture as front and back contact, or interdigitated back contact solar cells. Indeed, small contact sizes and distance between contacts are preferred for improving transport of

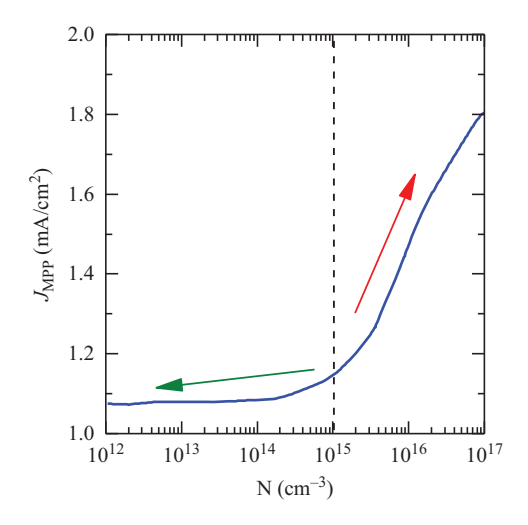


Figure 7.7 Intrinsic loss current density at maximum power point J_{MPP} as a function of the doping concentration N for ideal 110 μ m thick n-type solar cells under illumination with the AM 1.5 spectrum and 25°C. Green arrow indicates a slight J_{MPP} decrease for $N < 10^{15}$ cm⁻³. Red arrow indicates a significant J_{MPP} increase for $N > 10^{15}$ cm⁻³. J_{MPP} values are digitized from [125]

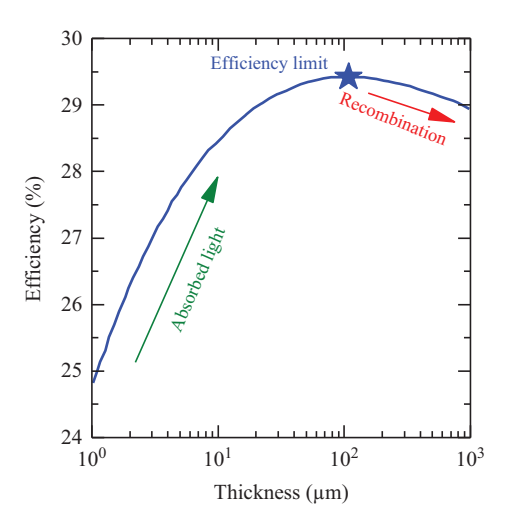


Figure 7.8 Efficiency as a function of the thickness for undoped c-Si cells under AM 1.5 illumination and 25°C. Green arrow indicates the increase of efficiency due to the improvement of absorbed light. Red arrow indicates the efficiency decrease due to intrinsic recombination. The efficiency limit is achieved for a thickness with the best trade-off: absorbed light vs recombination. Efficiency values are digitized from [125]

carriers. Therefore, the contact size/width and patterning resolution become relevant to minimize the path for collecting carriers and accordingly is a technological limitation for achieving the theoretical limiting efficiency.

The gap between the theoretical and practical efficiency limit for c-Si solar cells is expected to be reduced by: (i) using optimal light management at front and rear interface, (ii) using optimal passivation at interfaces (passivating contacts), (iii) using high-quality wafers with resistivity above $10~\Omega$ cm and with thickness around $110~\mu\text{m}$, iv) enabling smaller contacts and features.

7.4 Alternative carrier-selective contacts

7.4.1 Metal oxide and alkali metal-halogen compounds

Whereas direct metal contacts on silicon are straightforward and enable to use a simple window-layer stack with excellent transparency, the application of passivating contacts using doped silicon leads to complex processing and parasitically absorbing layers. There has therefore been since 2014 a resurgence of research aiming at applying metal compounds as carrier-selective contacts to silicon solar cells. Research has so far targeted mainly transparent materials, i.e. with a bandgap typically over 3 eV, with a few exceptions for use on the rear side of the device.

The most widely studied material families are the metal-oxide and the alkali (or alkaline-earth) metal-halogen compounds. The main material systems employed as selective contacts are shown in Figure 7.9. Using sub-stoichiometric molybdenum trioxide capped with ITO as a full-area hole-selective contact on the front side of the device, an efficiency of 23.5% was reached in 2019 [135] and further augmented to 23.8% in 2022 [136]. Conversely, using a titanium dioxide-lithium fluoride stack capped with aluminium as a partial-area electron-selective contact on the rear-side of the device, an efficiency of 23.1% was reached in 2018 [137]. These results were at that time very promising considering the little history for these approaches.

I	II		III	IV	V	VI	VII		VIII		I	II	III	IV	V	VI	VII	VIII
Н	Alkali/alkaline-earth																	Не
Li	Ве	1			Halogen Metal cation (hole contact)								В	С	N	0	F	Ne
							ation (el	`			-					_		
Na	Mg	,			IVICU	ai cati	on (c	icctio	ii coii	iact)	_		Al	Si	P	S	C1	Ar
K	Ca		Sc	Ti	V	Cr	Mn	Fe	Со	Ni	Cu	Zn	Ga	Ge	As	Se	Br	Kr
Rb			Y	Zr	Nb	Mo	Тс	Ru	Rh	Pd	Ag	Cd	In	Sn	Sb	Те	I	Xe
Cs	Ва	*	Lu	Hf	Та		Re	Os	Ir	Pt	Au	Hg	T1	Pb	Bi	Po	At	Rn
Fr	Ra	**	Lr	Rf	Db	Sg	Bh	Hs	Mt	Ds	Rg	Cn	Nh	Fl	Mc	Lv	Ts	Og

Figure 7.9 Chemical elements used in carrier-selective contacts based on metal oxide and alkali metal-halogen compounds

7.4.1.1 Hole-selective contacts

High-workfunction metal oxides using a fully oxidized metal cation from column VI of the periodic table (CrO_3 , MoO_3 , and WO_3) are the most studied materials, together with V_2O_5 . When stoichiometric, they typically are insulators with a bandgap over 3 eV and a work function over 6 eV. Nevertheless, they naturally tend to be sub-stoichiometric, which reduces slightly their workfunction while enabling conductivity. When deposited on silicon, this high workfunction induces a strong bending of the conduction and valence bands, leading to accumulation for a p-type wafer (inversion for an n-type wafer) thus inducing hole selectivity. Thermal evaporation is the most widely used deposition technique; reactive sputtering so far yielded underwhelming performances, yet remarkable performance was obtained with V_2O_5 deposited by ALD [138]. Since they do not provide efficient surface passivation, an additional passivation layer (most typically amorphous silicon) is inserted between the metal oxide and the silicon wafer.

Deposition conditions as well as pre- or post-deposition treatments prove to be very critical to the performance of the contact. MoO₃ was shown to be sensitive to reduction, which typically can be caused by hydrogen effusion from the passivating amorphous silicon layer. Preventing such effusion is thus critical, e.g. by reducing the H content of the a-Si layer prior to MoO₃ deposition, or by maintaining the thermal budget following MoO₃ deposition below 150°C. Additionally, plasma treatments prior to MoO₃ deposition were shown to enable an increase in performance together with a reduction of the required MoO₃ thickness [139]. Even more striking is the case of titanium dioxide, traditionally used as electron-selective contact as discussed in the following, but which can behave as a hole-selective contact when processed with dedicated approaches [140].

Several approaches were therefore investigated to implement metal-oxide hole-selective layers, but without a clear demonstration of improved performance compared to traditional contacts. Parasitic light absorption, and significant contact resistance impede the overall solar cell performance. Besides, the need for a dedicated passivation layer makes processing similarly complicated as for standard doped-silicon-based contacts.

7.4.1.2 Electron-selective contacts

A broader variety of materials were used as electron-selective contacts, mostly relying on a low workfunction. Alkali or alkaline-earth metal halides typically provide such low work function. They however function as efficient electron-selective contacts only when combined with a low-workfunction metal such as aluminum or magnesium. Mostly used metal-oxides are titanium dioxide and zinc oxide, also combined with a low-workfunction metal, or even a lithium-fluoride/aluminium stack. Although electron selectivity has long been attributed to the combination of adequate conduction band alignment and strong valence-band mismatch, this is being reassessed following the aforementioned discovery that TiO₂ can also be an efficient hole-selective contact. Part of the selectivity is therefore thought to stem from the electrode (or electrode stack). The absence of transparent electrodes with a low workfunction prevents to use these materials on the front side of the device.

A higher level of passivation was shown when using metal-oxides as electron-selective contacts than in the hole-selective contact case. This probably stems from the use of deposition techniques including some hydrogen, such as ALD or CVD. Nevertheless, dedicated passivation layers, such as a-Si:H or SiO_x:H are generally included for higher passivation. Performance stability is an active research topic, with some of the best-performing strategies degrading rapidly even without strong external stress [141]. Furthermore, best-performing contacts require an elaborate stack of layers with nanometric thicknesses, with similar or higher complexity compared to traditional contacts.

Alternative materials being evaluated include metal nitrides such as tantalum nitride or titanium nitride. Using the latter, working solar-cell devices were demonstrated with a single TiN layer as electron-selective contact. Efficiency was however not as high as when using more complex stacks.

7.4.1.3 Perspectives

Multiple strategies were investigated to implement non-silicon-based contacts in silicon solar cells. Remarkable performance was demonstrated in a short timeframe. Nevertheless, similarly to traditional contact strategies, high performance comes at the cost of relatively high complexity. There is nevertheless still a wide range of candidate materials that has not yet been widely investigated. Most studied materials so far were inspired from the organic semiconductor field (photovoltaics as well as light-emitting diodes). The field of wide-band-gap semiconductors remains to be investigated in detail, and the very promising results recently achieved with nanocrystalline silicon carbide suggest that this is highly relevant [26]. Indeed, the combination of a wide band gap and efficient por n-type doping is anticipated to be key in enabling a given material to act as an efficient carrier-selective contact in silicon solar cells. In this framework, the perovskite-oxide, III-V or II-VI families include very attractive materials. With these, dedicated substrates and growth techniques are however required to ensure sufficient material quality, making a direct use as contact in silicon devices unpractical. In parallel, numerous novel semiconductors are being predicted and experimentally demonstrated, widening further the possibilities. To this regard, ternary nitrides offer underexplored space with promising properties such as dopability or defect tolerance. Considering the variety of materials available, high-throughput experimentation would likely be appropriate to scan the parameter space efficiently. Nevertheless, their efficient implementation as contacts in silicon solar cells is unlikely to be an easy task, making dedicated effort likely required to reach high performance. A fine balance between rapid exploration and detailed investigation will thus have to be found should such alternative approach be envisioned. That is worthwhile though since unveiling an easy-to-process contact material with improved transparency compared to doped silicon together with similar passivation, selectivity, and reliability would enable solar cells in mass production to reach efficiency values up to 27%, making this a gamechanger in the photovoltaics industry.

7.4.2 Organic carrier selective contacts

Besides inorganic carrier-selective contacts, substantial efforts have been put on researching the organic route since the first Si/organic solar cell reported in 1990 by Sailor *et al.* [142]. That device employed poly-(CH₃)₃Si-cyclooctatetraene as hole-selective contact, but later other materials were tested, such as poly[2-methoxy-5-(2-ethylhexyloxy)-1,4-phenylenevinylene] (MEH-PPV) [143], poly(3-hexylthiophene) (P3HT) [144], and poly(3,4-ethylenedioxythiophene) (PEDOT) [145]. Especially the last has received attention for its appealing basic properties such as optical transparency in its conducting state, high stability, moderate band gap, and low redox potential [146,147]. This material can be doped with polystyrene sulfonate (PSS) to form PEDOT:PSS, whose augmented conductivity is crucial in high performance Si/PEDOT:PSS solar cells [16]. So far, the highest conversion efficiency achieved in c-Si PV technology by means of an organic hole-selective contact (PEDOT:PSS) is 20.6% [148]. The architecture of such a device, dubbed *BackPEDOT*, essentially simplifies the rear side of the PERC architecture, and thus embodies the promise of a low-CAPEX organic route with FF > 80% and j_{sc} close to 39 mA/cm².

Passing to the electron-selective contacts, Buckminsterfullerene (C_{60}) [149] and Lewis base polymers [150] have been successfully integrated in c-Si solar cells. In the first case, C_{60} was doped with tetrabutyl ammonium iodide (C_{60} :TBAI) and deployed at the front side of a simple, double side flat c-Si solar cell, yielding an efficiency of 8.43%. In the latter case, branched polyethylenimine (b-PEI) as well as other Lewis base polymers were tested on double side textured c-Si heterojunction cells endowed with standard i/p hole-selective contact stack based on a-Si: H at the front side and a-Si:H surface passivation at the rear side. The device with 3-nm thick b-PEI film yielded an efficiency of 19.4%, mostly supported by state-of-the-art $V_{oc} = 720$ mV. As strong donor of electrons, b-PEI induces strong downward bending in c-Si, thus favoring electron transport.

Leveraging existing processes typical of PERC or FBC heterojunction architectures (e.g. diffusion, PECVD a-Si:H, sputtering, screen printing, etc.), organic charge-selective contacts hold the potential to simplify and/or make cheaper their fabrication. However, further advancement in this route demands research efforts not only for improving the conversion efficiency of organic/c-Si solar cells but also their stability against temperatures beyond 200°C, UV light, and oxygen [16].

7.5 Silicon-based tandem cells

As outlined above, silicon single-junction solar cells are currently dominating the photovoltaics market and are slowly reaching their practical limit in module efficiency. For a further drop in the levelized cost of solar energy, aiming for higher power conversion efficiency is an obvious path. Today, the only experimental demonstration of overcoming the single-junction detailed balance limit has been achieved by multijunction solar cell technology. Multijunction cells tackle the shortcoming that incident photons with an energy above bandgap lead to a dissipation of their excess energy into the lattice of the absorber as heat (thermalization).

By adding additional solar cells with higher bandgaps, the potential of the highenergy photons is harvested more effectively [151,152]. The simplest realization of this concept is a tandem solar cell. Here, a combination of two subcells shares the solar spectrum (see Figure 7.10) and, upon optimal choice of the bandgaps, this leads to higher power conversion efficiencies.

The two subcells can be combined in three ways (see Figure 7.11): (1) monolithic stacking, where the top cell is processed on top of the bottom cell. This leads to two-terminal (2T) tandems. Both cells then share the top and bottom electrodes, and they are interconnected by a recombination layer. Ideally, this interlayer behaves like an ohmic contact with a low (vertical) series resistance. Due

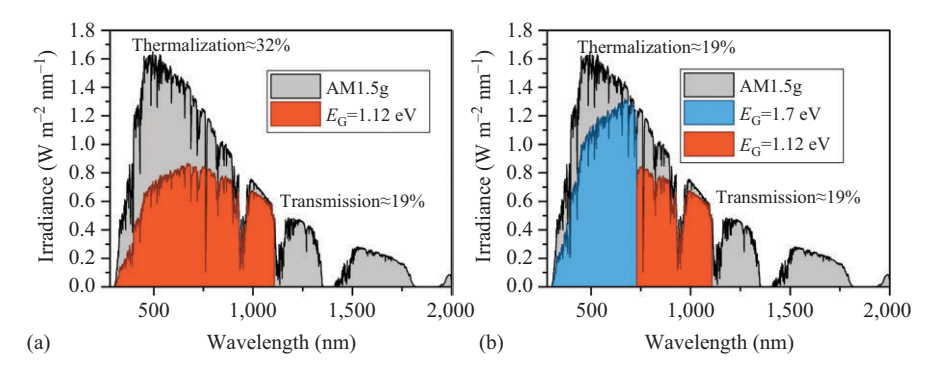


Figure 7.10 Fraction of the AM1.5g spectrum which can be used in a single-junction solar cell with a bandgap of 1.12 eV such as silicon (A) or in a multijunction solar cell where materials with bandgaps of 1.7 eV and 1.12 eV are combined (B). In this specific single-junction solar cell, around 19% of the incoming power is lost due to transmission (photons with energies lower than the lowest bandgap) whereas 32% is lost due to thermalization. In tandem solar cells, high energy photons are absorbed in the wide bandgap top cell, which reduces the amount of thermalization. For this specific combination of bandgaps, the losses due to thermalization are reduced to 19%

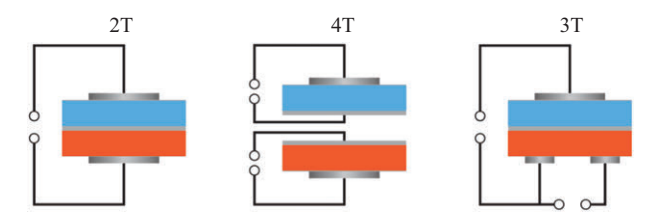


Figure 7.11 Schematics of different tandem architectures, where the blue subcell is the top cell and the orange cell represents the bottom cell: 2T, 4T, and 3T

to the series connection, the voltages of the subcells add up and the photocurrent of the device is limited by the lower one of the photocurrents generated in the two subcells. (2) Mechanical stacking resulting in four-terminal (4T) tandems, where both subcells are independent from each other and the top cell acts as an optical filter for the bottom cell. (3) Three-terminal (3T) interconnection combines the characteristics of both 2T and 4T tandems, in that the device stack is monolithic, but the two subcells can still be controlled independently [40].

Figure 7.12 shows the detailed balance efficiency limit of 2T and 4T tandem solar cells as a function of the top- and bottom cell bandgap under AM1.5g illumination (calculated according to [151]). The independent operation of the subcells in the 4T architecture enables a broad window where high efficiencies can be achieved. The highest PCE of 46.1% is achieved when materials with bandgaps of 1.73 eV and 0.93 eV are combined. If silicon with a bandgap of 1.12 eV is used as a bottom cell, the highest PCE of 45.2% can be achieved if the top cell has a bandgap of 1.82 eV. In the 2T architecture, the output current is limited by the subcell with the lowest current generation. Thus, in the best case, both cells generate the same current at their respective maximum power point (same $J_{\rm MPP}$ for both subcells). As the amount of generated current strongly depends on the subcell bandgap, only a narrow window exists where high PCEs can be achieved. The highest PCE of 45.7% is achieved when bandgaps of 1.60 eV and 0.94 eV are combined. If silicon is used as bottom cell, the highest efficiency of 45.0% is achieved when combining it with a material having a bandgap of 1.73 eV.

7.5.1 Perovskite-silicon tandems

As seen in Figure 7.12, a good tandem partner for Si cells would have a bandgap of around 1.7 eV [153]. Ideally, the cost of the top cell should be minimal, such that the efficiency gain leads to a reduced levelized cost of electricity. On top, the

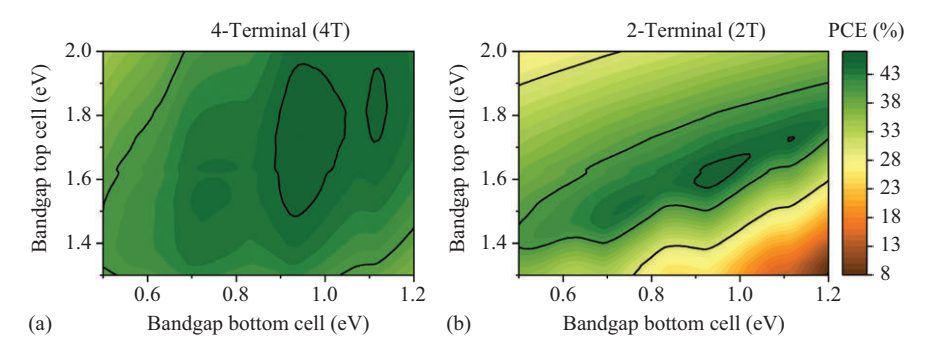


Figure 7.12 Detailed balance limit of tandem solar cells in 4T (A) and 2T (B) architecture as a function of the top- and bottom cell bandgap. The black lines indicate a PCE increment of 5% (i.e. 5%, 10%, 15%, etc.). The detailed balance limit is calculated according to [151] using the AM1.5g spectrum

processing complexity of the top cell should be minimal, to facilitate integration into existing Si cell production lines with a minimal number of barriers for the factories. Metal-halide perovskite semiconductors have the potential to combine all these aspects: favorable optoelectronic properties at low processing temperatures of around 100°C [154], low sub-bandgap absorption [155], a wide variety of fabrication methods and a variable bandgap. Their general compositional formula is ABX₃, where A denotes a monovalent cation (usually mixed organic/inorganic atoms or small molecules), B is a metal (mostly Pb, Sn or a mixture), and X denotes a halide anion (I, Br, Cl or a mixture thereof). For the A site, a wide variety of combinations can be found in literature [13]. For highly efficient perovskite/Si tandem solar cells, the organic cations formamidinium, methylammonium, and caesium have been used in mixtures, while the bandgap (optimized at 1.66–1.68 eV [156,157]) has been mostly controlled by the iodide-to-bromide ratio in the composition [158].

The first functional 2T perovskite-silicon tandem solar cell was published by Mailoa *et al.* in 2015. The combination of a standard n-type back surface field (BSF) silicon cell with a perovskite (MAPbI₃) top cell in n-i-p configuration (where the electron-selective layer was deposited first, followed by the intrinsic perovskite and then the hole extraction layer) enabled a PCE of 13.7%. Later in 2015, Albrecht *et al.* used SnO₂ deposited via atomic layer deposition (ALD) as the perovskite cell's n-contact, which was deposited at temperatures below 120°C. This allowed to fabricate tandem solar cells with silicon heterojunctions (SHJ) as bottom cells. The so fabricated tandem solar cell improved the PCE to a stabilized value of 18.1%.

Since this achievement, the majority of highly efficient (>25%) tandem solar cells were fabricated on SHJ solar cells on (n)c-Si wafers. Furthermore, following a publication by Bush *et al.*, in which the perovskite is deposited on the hole-selective layer and the electron contact contained a SnO₂ buffer layer [159], most perovskite-silicon tandems employ this "inverted" p-i-n perovskite cell architecture.

Usually, silicon bottom cells have textured surfaces to reduce reflection losses. However, the several micrometre high pyramids are not compatible with solution processing of the perovskite, which is an order of magnitude thinner than the height of these pyramids. Sahli et al. presented a conformal deposition method for perovskites, which enabled the utilization of silicon bottom cells with textured front sides [160]. The reduced reflection enabled high photogenerated current densities in the subcells and with that a high j_{SC} in the tandem solar cell. The certified 25.2% were published in 2018. Afterwards, Al-Ashouri and Köhnen et al. optimized the perovskite composition, introduced new hole-selective materials, namely selfassembled monolayers (SAMs) and carried out further optical optimizations, thereby increasing the power conversion efficiency to 29.2% [161,162]. The optical cell design was further optimized with a nanotextured interconnection layer by Tockhorn and Sutter et al., enabling a certified efficiency of 29.8% [163,164]. In 2022, EPFL and CSEM announced a certified efficiency of 31.3% on silicon with textured front side and 30.9% using a planarized silicon front side. Later that year, HZB achieved a certified efficiency of 32.5% on a planar silicon front side by

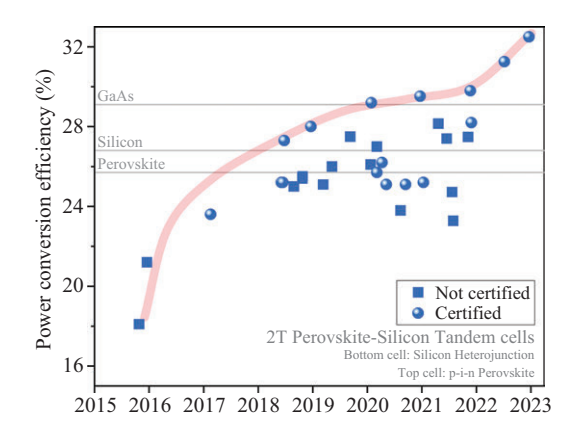


Figure 7.13 Best power conversion efficiencies of two-terminal perovskite-silicon tandem solar cells. The red line is a guide to the eye. The gray horizontal lines are for reference and indicate record efficiencies of other, single junciton technologies (non-concentrator) under global AM1.5 spectrum: GaAs (thin film cell) with 29.1%, silicon (crystalline cell) with 26.7% and perovskite (thin film) with 25.7% [5,8]

optimizing interfaces and optical modifications at the front side of the perovskite cell [194]. These values not just surpass the highest single-junction solar cell (GaAs, 29.1%) and even the (Auger-corrected) detailed-balance limit of silicon single-junction solar cells but approach the highest overall 2T tandem efficiency of 32.9% for GaInP/GaAs [10.1002/pip.3646]. These high efficiencies were achieved mostly on n-type silicon.

This impressively rapid improvement of the PCE for perovskite-silicon tandem solar cells is yet unique among all solar cell technologies. A plot of the time evolution of best power conversion efficiencies is depicted in Figure 7.13. With increasing PCE, the scientific focus in the community shifts more toward increasing the stability of the tandem cells, dealing with the sensitivity of perovskite layers against heat and moisture and also investigating the behaviour under real-world conditions [157,165]. Furthermore, the implementation of "drop-in tandem upgrades" for existing PERx technologies can be expected to become an important topic, as discussed by Messmer *et al.* based on simulations [166]. First such proof-of-concept perovskite/PERC/POLO tandems have been realized just recently in a collaboration between Helmholtz-Zentrum Berlin and ISFH [167].

7.5.2 III–V/Silicon tandems

While perovskite-silicon solar cells are today's shooting star, when it comes to tandem solar cells, III–V/silicon tandems have a much longer history starting in the 1990s. Today, III–V/Si cells also hold the efficiency record for tandem cells on silicon under the unconcentrated AM1.5g spectrum, with 32.8% in a mechanically stacked 4T GaAs/Si tandem [168]. Furthermore, 2T wafer bonded as well as 4T mechanically stacked

triple-junction cells—GaInP/GaInAsP//Si and GaInP/GaAs//Si stacks, respectively—have been demonstrated with identical efficiencies of 35.9% [5,168,169].

In these cells, knowledge gained in the fabrication of III–V compound semiconductor-based multijunction cells for space and concentrator PV applications is transferred for fabricating tandems and triple junction cells on silicon. Major advantages of the III–V semiconductors are (i) their direct band gap, thus the possibility to use thin film absorbers, and (ii) the wide range of band gaps that can be covered by variations in stoichiometry, especially when not only binary alloys such as GaAs, but also ternary and even quaternary alloys are considered [170]. For example, alloying Ga with indium (In) and arsenic (As) or phosphorous (P), a band gap range from \sim 1.4 to \sim 2.3 eV can be covered. This range extends even well beyond the most interesting region for both 2T and 4T tandems on silicon bottom cells, cf. Figure 7.12.

Historically, much of the development of III–V-based tandems on wafers was carried out on gallium arsenide (GaAs) and germanium (Ge) substrates. However, the shortage and relatively high cost of Ge makes this a difficult material for large-scale deployment of PV. Therefore, the focus has shifted to using silicon as an alternative substrate; it is worth mentioning that this is also an interesting field of research for the microelectronics industry [171].

As with perovskite-Si tandems, also III–V-Si devices can be broadly classified into 2T and 4T devices, and they can be fabricated either by direct growth of the III–V films on the Si wafer, or by mechanical stacking.

For fabricating 2T tandems by direct growth of III-V on Si, yielding 2T tandems, the challenge lies in achieving high quality of material both at the growth interface and in the III-V film's bulk. This requires the epitaxial growth of an antiphase-free nucleation layer, using MBE and/or MOCVD techniques. Typically, GaP is grown since it is lattice-matched to silicon with a suitable surface reconstruction. Epitaxy could be achieved with sufficient quality [172,173], but special offcut and polished Si wafers had to be used. Thus, this is approach is not compatible with usual saw damage etched PV-grade silicon, much less with textured wafers. Continuing with the growth of the actual top cell absorber layer, a second challenge arises: to achieve suitable band gaps, the ternary alloys GaAsP or GaInP should be used (e.g., $GaAs_{0.8}P_{0.2}$ has a band gap of $\sim 1.66eV$). However, the lattice constants of these materials are larger than that of Si by several percent. In addition, the thermal expansion coefficients of the materials differ significantly. Thus, such heteroepitaxial growth will induce the formation of dislocations, which are detrimental to the electronic quality. To tackle this issue, the so-called metamorphic epitaxy, which is key to record efficiencies in III-V multijunction technology, has been applied for III-V on Si growth. However, the device performances achieved so far are rather moderate, at 23.1% for a GaAsP/Si 2T tandem cell [5,174] and 25.9% for a GaInP/GaAs/Si monolithic 2T triple junction cell [175]. In the latter cell, a graded $Al_xGa_{1-x}As_vP_{1-v}$ buffer layer with a gradual increase of the band gap was used for the metamorphic transition on the Si wafer. Still, the efficiency for this quite complicated device stays below the Si single junction record.

The limitations in the direct growth approach render bonding of III-V on Si for 2T tandems an interesting option: Here, the III-V top and Si bottom cells are

fabricated separately, alleviating problems due to process incompatibilities, cross contamination, etc. For 2T tandem cells, the III-V cells are then attached to their Si partner by mechanical bonding, and the support used in III–V growth is removed. The bonding step at the same time forms an electrical series interconnection; in literature, the bonding interface is often denoted with a double slash, "//," to distinguish it from interfaces formed by layer growth. The main challenges for the bonding approach are the need for very flat/polished interfaces, incompatible with texture, and the development of various process steps for: (i) surface cleaning to remove any residual oxides or contaminations and promote adhesion; (ii) homogeneous, well-aligned bonding also on large areas; (ii) re-use of the wafer on which the III-V cells have been grown. If suitable, cost efficient solutions can be developed, this technology has significant potential: while in tandem cells, moderate efficiencies of 21.1% have been demonstrated using AlGaAs//Si [176], a waferbonded GaInP/GaInAsP//Si 2T triple junction cell has shown an efficiency of 35.9% $(j_{sc} 13.1 \text{ mA/cm}^2, V_{oc} 3.25 \text{ V}, \text{ FF } 84.3\%) [169]. \text{ Among others, a TOPCon bottom}$ cell, double antireflective coating and a nanostructured diffractive rear-side grating have been used to maximize performance. This is today's world record efficiency for such devices, on par with a mechanically stacked 4T triple junction device.

As an alternative to bonding, the so-called "smart stack" [177] has been developed: it uses transparent conductive adhesives for subcell interconnection into 2T III–V-Si multijunction cells and has recently shown interesting potential, with up to 30.8% efficient InGaP/AlGaAs//Si triple junction cells in 2T configuration [178].

Another classical option is to process both subcells into full cells, with two terminals each, and then form a mechanical stack using transparent, refractive indexmatched and electrically insulating glue. This yields III–V on Si 4T tandems. The same advantages and caveats as for such 4T tandems with other combinations of absorber materials apply, i.e. briefly: potentially better energy yield due to better resilience toward non-optimal illumination spectra vs. additional parasitic absorption in the two additional contact stacks consisting of laterally conductive layers and metallization grids. Despite the latter disadvantage, a 35.9% efficient GaInP/GaAs//Si triple junction 4T cell could be fabricated. The other parameters were: V_{oc} 2.52 and 0.681 V in the III– V top and Si bottom cell, respectively, j_{sc} 13.6 and 11.0 mA/cm², FF 87.5 and 78.5% [168]. In the same publication, a 32.8% 4T tandem cell with GaInP and Si absorbers was demonstrated. Furthermore, the paper contains a cost analysis which reveals the biggest challenge in III-V/Si technology: the use of costly GaAs wafer substrates and MOVBE epitaxy processes for the III-V solar cell stack. Thus, techniques for more than 100 substrate reuses as well as faster deposition techniques, such as high-growthrate MOVPE, close-space vapor transport and hydride vapor phase epitaxy (HVPE) need to be developed further to make III-V on Si multijunctions a viable option.

7.6 Projections

The energy transition from fossil fuels to renewable energy is one of the biggest challenges mankind faces nowadays. The last two decades have seen a continued exponential growth of renewable energy technologies such as wind and solar [179],

contributing to the energy mix of several countries in appreciable percentages [180]. This development mitigates climate change, supports the UN sustainable development goals [181], and is driven by the electrification of society. In this age of information and digitalization, electricity is the most versatile energy carrier, serving the built environment, industrial processes, electrical mobility, and sustainable farming while enabling smart data connection.

The electrical energy system of today transforms the chemical energy of fossil fuels into thermal, mechanical, and ultimately electrical energy. This system is centralized with a few power plants that unidirectionally distribute electricity from very high-voltage levels down to medium and low-voltage levels. For its reliance on fossil fuels and related CO₂ emissions, today's electrical energy system is one of the major causes of climate change. Most of the cumulative installed power of wind and solar can be thus far ascribed to GW-scale onshore wind [182] and PV plants [183] that are co-existing with fossil fuel and nuclear power plants. It is undeniable that PV modules based on p-type c-Si technology have played a crucial role in such growth, benefitting from an industrial maturity that has steadily increased the conversion efficiency while driving down the costs. Owing to this success, the power plant level LCOoE of solar electrical energy is today the lowest in many countries [184–186].

The generation of electricity from renewable energy sources can be achieved also at medium and low-voltage levels, that is, closer to local consumption. While the installation of onshore wind turbines is not always practical for issues related to wildlife safety, societal acceptance, and ecological impact [187], PV systems can be massively integrated in both urban and open environments with much lower societal and economic barriers. By 2050, more than 65% of the ever-growing global population will live in urban areas [188] resulting in two major challenges. First, cities will need more energy to satisfy their population's needs and, second, nearby rural areas will be primarily used for food production. In this respect, the generation of green electricity by means of PV systems will compete in both cities and rural areas with land scarcity.

PV systems based on n-type c-Si solar cell architectures will tackle these challenges by ensuring a continued increase in conversion efficiency by single-junction technology and, later, by embodying the ideal bottom sub-cell technology for future tandem PV modules. That is, given the same form factor and environmental conditions, n-type PV modules will exhibit higher annual energy density (kW h/m²) than their current p-type counterparts, for which either smaller form factors can be devised with similar energy output to current modules or standard form factors can be produced enabling intra-module customization and thus new applications. Owing to the higher conversion efficiency, the production in volumes of such n-type modules will further drive down the c-Si PV learning curve. At the same time, as n-type solar cells enable several new applications, e.g. environment-integration (EIPV), urban-integration (UIPV), and vehicle-integration (VIPV), customized n-type PV modules will also be produced with economic return.

Therefore, in future cities, the electricity-driven energy system will be fed by high-performance n-type PV systems that can pave every surface in the

environment providing useful green electricity for the sustainable electrification of society. Also, shade-resilient modules [189] integrated with storage of electrical or thermal energy and communication capabilities will constitute the so-called *PV-based intelligent energy agents*. These will cover the whole conversion chain from photons to electrons to bits, marking the advent of the photovoltatronics age [190]. At the same time, as n-type PV systems can deliver higher performance than current p-type based ones, more powerful PV plants occupying less space will be realized for a more granular green electricity generation in the vicinity of cities. Finally, diverse and powerful EIPV systems, such as floating PV or agri-PV systems, will be installed competing less for land or water otherwise needed for other utilizations.

With more than 700 GW_p cumulatively installed in 2020 [191] and, according to projections [192], more than 900 GW_p cumulatively installed in 2021, PV systems installations are well on track to break the TW_p scale by 2022. These formidable numbers are due to PERX/iTOPCon architectures, that dominate the market with 80% share [12], and the arising of silicon heterojunction (HTJ) technology, whose market share is expected to grow well above 15% by 2030.

7.7 Summary

In this chapter, we have reviewed candidates for further enhancement of cell efficiencies beyond those of today's mainstream PERC cells, with a focus on technological aspects rather than, e.g. cost. Regarding silicon single junctions, the prevalent theme is the use of carrier-selective passivating contacts, CSPCs. Of these, silicon heterojunction and polysilicon-on-silicon oxide (TOPCon/POLO) are most advanced and have enabled record high efficiencies above and close to 26%, respectively, on n-type silicon wafers. Further important topics are bifacial cell designs, which can be applied to different PV technologies. Single-side efficiencies above 25% have been achieved on bifacial TOPCon and bifacial SHJ solar cells. With proven bankability, bifacial PV products can be expected to gain more momentum in future development. In contrast, contacts based on metal compounds have yielded remarkable results in the last decade, yet failing to clearly evidence a significant advantage compared to the ones based on silicon. Further research is needed to unravel the material combination that would enable the long-awaited ultimate passivating contact for Si solar cells.

The second major topic are tandem and multijunction cells. This is the technology to move beyond the ultimate efficiency barrier of 29.4% for silicon PV and indeed, efficiencies well above 29% have been demonstrated in the lab for Si-based tandems. We have reviewed the current state of the art in lead halide perovskite-silicon tandems as well as III–V/silicon tandems. The former have reached a record PCE of 32.5% in monolithically integrated 2-terminal tandems, while III–V/Si 2T tandems currently stand at 23.4%. However, in III–V-Si devices, the number of absorbers has already been increased further, to three: in triple junction III–V/III–V/Si cells, PCEs of 35.9% have been realized with both 2T and 4T architectures.

With a substantially higher cost for the III–V technology as compared to perovskites, but still inferior long-term stability in perovskites, as well as challenges in upscaling for both technologies, it remains to be seen which one of these technologies will gain an advantage. It should be mentioned that an important difference between reported silicon single junction and tandem/multijunction record devices is the cell area: while the single junction Si record devices have "industrial-size" active areas of several tens of cm² or even full wafers, record tandem cells are labscale 1–4 cm². Thus, up-scaling of tandem cells will remain an important topic in the near future.

At any rate, it can be expected that the exponential growth of PV as well as the diversity of applications (utility, rooftop and BIPV, agri-PV, etc.) will create ample opportunity for the market entry of quite a few of the mentioned technologies, and even for entirely new concepts such as three-terminal tandems or, at the module level, integrated PV and storage systems.

References

- [1] Snapshot of Global PV Markets 2021. IEA-PVPS; 2021, p. 22. [cited 2022 Feb 28]. Available from: https://iea-pvps.org/snapshot-reports/snapshot-2021/
- [2] Niewelt T, Schön J, Warta W, Glunz SW, and Schubert MC. Degradation of crystalline silicon due to boron–oxygen defects. *IEEE J Photovolt.* 2017; 7(1):383–98.
- [3] Wurfel U, Cuevas A, and Wurfel P. Charge carrier separation in solar cells. *IEEE J Photovolt.* 2015;5(1):461–9.
- [4] Rau U and Kirchartz T. Charge carrier collection and contact selectivity in solar cells. *Adv Mater Interfaces*. 2019;6:1900252.
- [5] Green MA, Dunlop ED, Siefer G, *et al.* Solar cell efficiency tables (version 61). *Prog Photovolt Res Appl.* 2023;31(1):3–16.
- [6] Yamamoto K, Yoshikawa K, Uzu H, and Adachi D. High-efficiency heterojunction crystalline Si solar cells. *Jpn J Appl Phys.* 2018;57(8S3): 08RB20.
- [7] Yoshikawa K, Kawasaki H, Yoshida W, *et al.* Silicon heterojunction solar cell with interdigitated back contacts for a photoconversion efficiency over 26%. *Nat Energy.* 2017;2(5):17032.
- [8] At 26.81%, LONGi sets a new world record efficiency for silicon solar cells. [cited 2023 Jan 05]. Available from: https://www.longi.com/en/news/propelling-the-transformation/
- [9] LONGi announces new world record cell efficiencies. [cited 2023 Jan 05]. Available from: https://www.longi.com/en/news/new-record-cell-for-hjt/
- [10] Taguchi M, Terakawa A, Maruyama E, and Tanaka M. Obtaining a higher Voc in HIT cells. *Prog Photovolt Res Appl.* 2005;13(6):481–8.
- [11] Haschke J, Dupre O, Boccard M, and Ballif C. Silicon heterojunction solar cells: recent technological development and practical aspects from lab to industry. *Sol Energy Mater Sol Cells*. 2018;187:140–53.

- [12] ITRPV Roadmap, 12 ed. VDMA, 2021.
- [13] Jošt M, Kegelmann L, Korte L, and Albrecht S. Monolithic perovskite tandem solar cells: a review of the present status and advanced characterization methods toward 30% efficiency. *Adv Energy Mater*. 2020;10(26): 1904102.
- [14] De Wolf S, Descoeudres A, Holman ZC, and Ballif C. High-efficiency silicon heterojunction solar cells: a review. *Green.* 2012;2:7–24.
- [15] Battaglia C, Cuevas A, and Wolf SD. High-efficiency crystalline silicon solar cells: status and perspectives. *Energy Environ Sci.* 2016;9(5):1552–76.
- [16] Liu Y, Li Y, Wu Y, *et al.* High-efficiency silicon heterojunction solar cells: materials, devices and applications. *Mater Sci Eng R Rep.* 2020;142:100579.
- [17] Sark WGJHM, van Korte L, and Roca F, editors. *Physics and Technology of Amorphous-Crystalline Heterostructure Silicon Solar Cells*, 2011th ed. New York, NY: Springer; 2011. 596 p.
- [18] Korte L and Schmidt M. Doping type and thickness dependence of band offsets at the amorphous/crystalline silicon heterojunction. *J Appl Phys.* 2011;109(6):063714.
- [19] Fuhs W, Niemann K, and Stuke J. Heterojunctions of amorphous silicon and silicon single crystals. In: *Tetrahedrally Bonded Amorphous Semiconductors*. Yorktown Heights, 1974, pp. 345–50 (American Institute of Physics Conference Proceedings; vol. 20).
- [20] Tanaka M, Taguchi M, Matsuyama T, *et al.* Development of new a-Si/c-Si heterojunction solar cells: ACJ-HIT (artificially constructed junction-heterojunction with intrinsic thin-layer). *Jpn J Appl Phys.* 1992;31:3518–22.
- [21] Yano A, Tohoda S, Matsuyama K, *et al.* 24.7% Record efficiency HIT[®] solar cell on thin silicon wafer. In: *28th Eur Photovolt Sol Energy Conf Exhib.*, 2013 Nov 22, pp. 748–51.
- [22] Taguchi M. Review—Development history of high efficiency silicon heterojunction solar cell: from discovery to practical use. *ECS J Solid State Sci Technol.* 2021;10(2):025002.
- [23] Masuko K, Shigematsu M, Hashiguchi T, *et al.* Achievement of more than 25% conversion efficiency with crystalline silicon heterojunction solar cell. *IEEE J Photovolt.* 2014;4(6):1433–5.
- [24] Chunduri SK and Schmela M. *Heterojunction Solar Technology*, 2020 ed. Düsseldorf, Germany: TaiyangNews, 2020. Available from: https://taiyangnews.info/reports/heterojunction-solar-technology-2020-report/
- [25] Boccard M and Holman ZC. Amorphous silicon carbide passivating layers for crystalline-silicon-based heterojunction solar cells. *J Appl Phys.* 2015; 118(6):065704.
- [26] Köhler M, Pomaska M, Procel P, *et al.* A silicon carbide-based highly transparent passivating contact for crystalline silicon solar cells approaching efficiencies of 24%. *Nat Energy.* 2021;6(5):529–37.
- [27] Mazzarella L, Kirner S, Stannowski B, Korte L, Rech B, and Schlatmann R. p-type microcrystalline silicon oxide emitter for silicon heterojunction

- solar cells allowing current densities above 40 mA/cm². *Appl Phys Lett.* 2015;106(2):023902.
- [28] Seif JP, Descoeudres A, Filipič M, *et al.* Amorphous silicon oxide window layers for high-efficiency silicon heterojunction solar cells. *J Appl Phys.* 2014;115(2):024502.
- [29] Cuevas A and Yan D. Misconceptions and misnomers in solar cells. *IEEE J Photovolt*. 2013;3(2):916–23.
- [30] Bivour M, Schröer S, Hermle M, and Glunz SW. Silicon heterojunction rear emitter solar cells: less restrictions on the optoelectrical properties of front side TCOs. *Sol Energy Mater Sol Cells*. 2014;122:120–9.
- [31] Koida T, Ueno Y, and Shibata H. In₂O₃-based transparent conducting oxide films with high electron mobility fabricated at low process temperatures. *Phys Status Solidi A*. 2018;215(7):1700506.
- [32] Meza D, Cruz A, Morales-Vilches AB, Korte L, and Stannowski B. Aluminum-doped zinc oxide as front electrode for rear emitter silicon heterojunction solar cells with high efficiency. *Appl Sci.* 2019;9(5):862.
- [33] Morales-Vilches AB, Cruz A, Pingel S, *et al.* ITO-free silicon heterojunction solar cells with ZnO:Al/SiO₂ front electrodes reaching a conversion efficiency of 23%. *IEEE J Photovolt.* 2019;9(1):34–9.
- [34] Barraud L, Holman ZC, Badel N, *et al.* Hydrogen-doped indium oxide/indium tin oxide bilayers for high-efficiency silicon heterojunction solar cells. *Sol Energy Mater Sol Cells.* 2013;115:151–6.
- [35] Yu J, Li J, Zhao Y, *et al.* Copper metallization of electrodes for silicon heterojunction solar cells: process, reliability and challenges. *Sol Energy Mater Sol Cells*. 2021;224:110993.
- [36] Yao Y, Papet P, Hermans J, *et al.* Module integration of solar cells with diverse metallization schemes enabled by SmartWire Connection Technology. In: *2015 IEEE 42nd Photovoltaic Specialist Conference (PVSC)*, 2015, pp. 1–5.
- [37] Geissbühler J, Faes A, Lachowicz C, Ballif C, and Despeisse M. Metallization techniques and interconnection schemes for high efficiency silicon heterojunction PV. *PV Tech.* 2017;37:61–9.
- [38] Louwen A, van Sark W, Schropp R, and Faaij A. A cost roadmap for silicon heterojunction solar cells. *Sol Energy Mater Sol Cells*. 2016;147: 295–314.
- [39] Tomasi A, Paviet-Salomon B, Jeangros Q, *et al.* Simple processing of back-contacted silicon heterojunction solar cells using selective-area crystalline growth. *Nat Energy.* 2017;2(5):1–8.
- [40] Tockhorn P, Wagner P, Kegelmann L, *et al.* Three-terminal perovskite/ silicon tandem solar cells with top and interdigitated rear contacts. *ACS Appl Energy Mater.* 2020;3(2):1381–92.
- [41] Long W, Yin S, Peng F, *et al.* On the limiting efficiency for silicon heterojunction solar cells. *Sol Energy Mater Sol Cells*. 2021;231:111291.

- [42] Richter A, Müller R, Benick J, *et al.* Design rules for high-efficiency both-sides-contacted silicon solar cells with balanced charge carrier transport and recombination losses. *Nat Energy.* 2021;6(4):429–38.
- [43] Haase F, Hollemann C, Schäfer S, *et al.* Laser contact openings for local poly-Si-metal contacts enabling 26.1%-efficient POLO-IBC solar cells. *Sol Energy Mater Sol Cells*. 2018;186:184–93.
- [44] Yablonovitch E, Gmitter T, Swanson RM, and Kwark YH. A 720 mV open circuit voltage SiOx:c-Si:SiOx double heterostructure solar cell. *Appl Phys Lett.* 1985;47(11):1211–3.
- [45] Lindholm FA, Neugroschel A, Arienzo M, and Ilies PA. Heavily doped polysilicon-contact solar. *IEEE Electron Device Lett.* 1985;6(7):363–5.
- [46] Yang G, Zhang Y, Procel P, Weeber A, Isabella O, and Zeman M. Poly-Si (O)x passivating contacts for high-efficiency c-Si IBC solar cells. *Energy Proc.* 2017;124:392–9.
- [47] Yang G, Guo P, Procel P, Weeber A, Isabella O, and Zeman M. Polycrystalline silicon-oxide films as carrier-selective passivating contacts for c-Si solar cells. *Appl Phys Lett.* 2018;112(19):1–6.
- [48] Stuckelberger J, Nogay G, Wyss P, *et al.* Passivating electron contact based on highly crystalline nanostructured silicon oxide layers for silicon solar cells. *Sol Energy Mater Sol Cells.* 2016;158:2–10.
- [49] Nogay G, Stuckelberger J, Wyss P, *et al.* Interplay of annealing temperature and doping in hole selective rear contacts based on silicon-rich silicon-carbide thin films. *Sol Energy Mater Sol Cells.* 2017;173:18–24.
- [50] Nogay G, Stuckelberger J, Wyss P, *et al.* Silicon-rich silicon carbide hole-selective rear contacts for crystalline-silicon-based solar cells. *ACS Appl Mater Interfaces*. 2016;8(51):35660–7.
- [51] Yang Q, Liu Z, Lin Y, *et al.* Passivating contact with phosphorus-doped polycrystalline silicon-nitride with an excellent implied open-circuit voltage of 745 mv and its application in 23.88% efficiency TOPCon solar cells. *Sol RRL*. 2021;5(11):2100644.
- [52] Yang G, Van de Loo B, Stodolny M, *et al.* Passivation enhancement of poly-Si carrier-selective contacts by applying ALD Al_2O_3 capping layers. *IEEE J Photovolt.* 2021;1–8.
- [53] van de Loo BWH, Macco B, Schnabel M, *et al.* On the hydrogenation of poly-Si passivating contacts by Al2O3 and SiNx thin films. *Sol Energy Mater Sol Cells.* 2020;215:110592.
- [54] Reichel, C. Müller, R. Feldmann, F. Richter, A. Hermle, M, and Glunz SW. Interdigitated back contact silicon solar cells featuring ion-implanted poly-Si/SiOx passivating contacts. In: *33th Eur Photovolt Sol Energy Conf Exhib EU PVSEC*, 2017;
- [55] Polzin JI, Feldmann F, Steinhauser B, Hermle M, and Glunz SW. Study on the interfacial oxide in passivating contacts. *AIP Conf Proc.* 2019;2147(1):040016.
- [56] Geerligs BLJ, Stodolny MK, Wu Y, et al. LPCVD polysilicon passivating contact. In: Workshop Cryst Silicon Sol Cells Modul Mater Process, 2016, 28–31.

- [57] Schmidt J, Peibst R, and Brendel R. Surface passivation of crystalline silicon solar cells: present and future. Sol Energy Mater Sol Cells. 2018;187:39–54.
- [58] Steinkemper H, Feldmann F, Bivour M, and Hermle M. Numerical simulation of carrier-selective electron contacts featuring tunnel oxides. *IEEE J Photovolt.* 2015;5(5):1348–56.
- [59] Peibst R, Romer U, Larionova Y, *et al.* Working principle of carrier selective poly-Si/c-Si junctions: Is tunnelling the whole story? *Sol Energy Mater Sol Cells.* 2016;158:60–7.
- [60] Rienäcker M, Merkle A, Römer U, *et al.* Recombination behavior of photolithography-free back junction back contact solar cells with carrier-selective polysilicon on oxide junctions for both polarities. *Energy Proc.* 2016:412–8.
- [61] Yang G, Ingenito A, Van Hameren N, Isabella O, and Zeman M. Design and application of ion-implanted polySi passivating contacts for interdigitated back contact c-Si solar cells. *Appl Phys Lett.* 2016;108(3):033903.
- [62] Upadhyaya AD, Ok Y, Chang E, *et al.* Ion-implanted screen-printed n-type solar cell with tunnel oxide passivated back contact. *IEEE J Photovolt.* 2016;6(1):153–8.
- [63] Kim H, Bae S, Ji K-sun, *et al.* Passivation properties of tunnel oxide layer in passivated contact silicon solar cells. *Appl Surf Sci.* 2017;409:140–8.
- [64] Moldovan A, Feldmann F, Zimmer M, Rentsch J, Benick J, Hermle M. Tunnel oxide passivated carrier-selective contacts based on ultra-thin SiO₂ layers. *Sol Energy Mater Sol Cells*. 2015;142:123–7.
- [65] Lozac'h M, Nunomura S, and Matsubara K. Double-sided TOPCon solar cells on textured wafer with ALD SiOx layer. Sol Energy Mater Sol Cells. 2020;207:110357.
- [66] Stuckelberger J, Yan D, Phang SP, Samundsett C, and Macdonald D. Industrial solar cells featuring carrier selective front contacts. Presented at 36th Eur Photovolt Sol Energy Conf Exhib. 2019;
- [67] Ding Z, Yan D, Stuckelberger J, *et al.* Phosphorus-doped polycrystalline silicon passivating contacts via spin-on doping. *Sol Energy Mater Sol Cells*. 2020;221:110902.
- [68] Tutsch L, Feldmann F, Polzin J, et al. Implementing transparent conducting oxides by DC sputtering on ultrathin SiOx/poly-Si passivating contacts. Sol Energy Mater Sol Cells, 2019;200:109960.
- [69] Hollemann C, Haase F, Schäfer S, Krügener J, Brendel R, and Peibst R. 26.1%-efficient POLO-IBC cells: quantification of electrical and optical loss mechanisms. *Prog Photovolt Res Appl.* 2019;27(11):950–8.
- [70] Wu W, Bao J, Ma L, *et al.* Development of industrial n-type bifacial topcon solar cells and modules Weiliang. In: *36th Eur Photovolt Sol Energy Conf Exhib Dev.*, 2019, October, pp. 2–5.
- [71] Chen Y, Chen D, Liu C, *et al.* Mass production of industrial tunnel oxide passivated contacts (i-TOPCon) silicon solar cells with average efficiency over 23% and modules over 345 W. *Prog Photovolt Res Appl.* 2019;27 (10):827–34.

- [72] Feldmann F, Bivour M, Reichel C, *et al.* Tunnel oxide passivated rear contact for large area n-type front junction silicon solar cells providing excellent carrier selectivity. *Sol Energy Mater Sol Cells.* 2014;131(Part A):46–50.
- [73] Ingenito A, Limodio G, Procel P, *et al.* Silicon solar cell architecture with front selective and rear full area ion-implanted passivating contacts. *Sol RRL*. 2017;1(7):1700040.
- [74] Ingenito A, Nogay G, Stuckelberger J, *et al.* Phosphorous-doped silicon carbide as front-side full-area passivating contact for double-side contacted c-Si solar cells. *IEEE J Photovolt.* 2019;9(2):346–54.
- [75] Chen J. The industrial application of n-type bifacial passivating-contact technology. In: 9th Int Conf Cryst Silicon Photovolt, 2019.
- [76] Feldmann F, Bivour M, Reicherl C, Hermle H, and Glunz SW. A passivated rear contact for high-efficiency. In: *Proc 29th Eur Photovolt Sol Energy Conf Paris Fr*, 2013.
- [77] Glunz SW, Feldmann F, Richter A, *et al.* The irresistible charm of a simple current flow pattern 25% with a solar cell featuring a full-area back contact. In: *Proc 31st Eur Photovolt Sol Energy Conf Exibition*, 2015, pp. 259–63.
- [78] Hermle M, Feldmann F, Eisenlohr J, *et al.* Approaching efficiencies above 25% with both sides-contacted silicon solar cells. In: *2015 IEEE 42nd Photovolt Spec Conf PVSC 2015*, 2015, pp. 8–10.
- [79] Krügener J, Haase F, Rienäcker M, Brendel R, Osten HJ, and Peibst R. Improvement of the SRH bulk lifetime upon formation of n-type POLO junctions for 25% efficient Si solar cells. *Sol Energy Mater Sol Cells*. 2017;173:85–91.
- [80] Morales-Vilches AB, Larionova Y, *et al.* ZnO:Al/a-SiOx front contact for polycrystalline-silicon-on-oxide (POLO) solar cells. *AIP Conf Proc.* 2018;1999(1):040016.
- [81] Nandakumar N, Rodriguez J, Kluge T, *et al.* Approaching 23% with large-area monoPoly cells using screen-printed and fired rear passivating contacts fabricated by inline PECVD. *Prog Photovolt Res Appl.* 2019; 27(2):107–12.
- [82] Nandakumar N, Rodriguez J, Kluge T, *et al.* 21.6% monoPoly TM cells with in-situ interfacial oxide and poly-Si layers deposited by inline PECVD. In: 2018 IEEE 7th World Conf Photovolt Energy Convers WCPEC 2018 Jt Conf 45th IEEE PVSC 28th PVSEC 34th EU PVSEC, 2018, 2048–51.
- [83] Reichel C, Müller R, Feldmann F, Richter A, Hermle M, and Glunz SW. Influence of the transition region between p- and n-type polycrystalline silicon passivating contacts on the performance of interdigitated back contact silicon solar cells. *J Appl Phys.* 2017;122(18):184502.
- [84] Richter A, Benick J, Müller R, *et al.* Tunnel oxide passivating electron contacts as full-area rear emitter of high-efficiency p-type silicon solar cells. *Prog Photovolt Res Appl.* 2018;26(8):579–86.

- [85] Richter A, Benick J, Feldmann F, Fell A, Hermle M, and Glunz SW. n-Type Si solar cells with passivating electron contact: identifying sources for efficiency limitations by wafer thickness and resistivity variation. *Sol Energy Mater Sol Cells*. 2017;173:96–105.
- [86] Römer U, Merkle A, Peibst R, *et al.* Ion-implanted poly-Si/c-Si junctions as a back-surface field in back-junction back-contacted solar cells. In: *Proc 29th Eur Photovolt Sol Energy Conf.*, 2014, October, pp. 1107–10.
- [87] Stodolny MK, Anker J, Geerligs BL, *et al.* Material properties of LPCVD processed n-type polysilicon passivating contacts and its application in PERPoly industrial bifacial solar cells. *Energy Proc.* 2017;124:635–42.
- [88] Cuevas A. The early history of bifacial solar cells. In: *Proceedings of the European Photovoltaic Solar Energy Conference*, Munich: WIP, 2005, pp. 801–5.
- [89] Chunduri SK and Schmela M. Bifacial Solar Technology 2021 Edition Part 1: Cells & Modules Report, 2021.
- [90] Liang TS, Pravettoni M, Deline C, *et al.* A review of crystalline silicon bifacial photovoltaic performance characterisation and simulation. *Energy Environ Sci.* 2019;12(1):116–48.
- [91] Ebong AU, Taouk M, and Wenham SR. A low cost metallization scheme for double sided buried contact silicon solar cells. *Sol Energy Mater Sol Cells*. 1994;31(4):499–507.
- [92] Wang X, Allen V, Vais V, et al. Laser-doped metal-plated bifacial silicon solar cells. Sol Energy Mater Sol Cells. 2014;131:37–45.
- [93] Chang Y-C, Wang S, Li S, Rong D, and Ji J. *Applications of simultaneously bifacial plating technology in bifacial solar cells. In: EU PVSEC* 2021, 2021, online.
- [94] Fu F, Feurer T, Jager T, *et al.* Low-temperature-processed efficient semi-transparent planar perovskite solar cells for bifacial and tandem applications. *Nat Commun.* 2015;6:8932.
- [95] Dupré O, Tuomiranta A, Jeangros Q, Boccard M, Alet P, and Ballif C. Design rules to fully benefit from bifaciality in two-terminal perovskite/silicon tandem solar cells. *IEEE J Photovolt*. 2020;1–8.
- [96] De Bastiani M, Mirabelli AJ, Hou Y, *et al.* Efficient bifacial monolithic perovskite/silicon tandem solar cells via bandgap engineering. *Nat Energy*. 2021;1–9.
- [97] Du D, Gao C, Zhang D, *et al.* Low-cost strategy for high-efficiency bifacial perovskite/c-Si tandem solar cells. *Sol RRL*. 2021;n/a(n/a).
- [98] Kim S, Trinh TT, Park J, *et al.* Over 30% efficiency bifacial 4-terminal perovskite-heterojunction silicon tandem solar cells with spectral albedo. *Sci Rep.* 2021;11(1):15524.
- [99] Chantana J, Kawano Y, Nishimura T, Mavlonov A, and Minemoto T. Optimized bandgaps of top and bottom subcells for bifacial two-terminal tandem solar cells under different back irradiances. *Sol Energy*. 2021;220:163–74.

- [100] Khan SN, Ge S, Gu E, *et al.* Bifacial Cu2ZnSn(S,Se)4 thin film solar cell based on molecular ink and rapid thermal processing. *Adv Mater Interfaces*. 2021;8:2100971.
- [101] Nishimura T, Chantana J, Mavlonov A, Kawano Y, Masuda T, and Minemoto T. Device design for high-performance bifacial Cu(In,Ga)Se2 solar cells under front and rear illuminations. *Sol Energy*. 2021;218:76–84.
- [102] Kopecek R and Libal J. Bifacial photovoltaics 2021: status, opportunities and challenges. *Energies*. 2021;14(8):2076.
- [103] Green MA, Wenham SR, Honsberg CB, and Hogg D. Transfer of buried contact cell laboratory sequences into commercial production. *Sol Energy Mater Sol Cells*. 1994;34(1–4):83–9.
- [104] Ebong AU. Double Sided Buried Contact Silicon Solar Cells, 1994.
- [105] Shenvekar S. N-Type TOPCon a Sign of the Times Jinko Solar, 2021.
- [106] Bhambhani A. CPVT Confirms LONGi Produced First Bifacial Monocrystalline Silicon PERC Solar Cell Exceeding 24% on Commercial Wafer Size, 2019.
- [107] Barth S, Doll O, Koehler I, *et al.* 19.4 Efficient bifacial solar cell with spinon boron diffusion. *Energy Proc.* 2013;38:410–5.
- [108] Dullweber T, Kranz C, Peibst R, *et al.* PERC+: industrial PERC solar cells with rear Al grid enabling bifaciality and reduced Al paste consumption. *Prog Photovolt Res Appl.* 2016;24(12):1487–98.
- [109] Ebong AU, Lee SH, Warta W, Honsberg CB, and Wenham SR. Characterization of high open-circuit voltage double sided buried contact (DSBC) silicon solar cells. *Sol Energy Mater Sol Cells*. 1997;45(3):283–99.
- [110] Heng J. B, Fu J, Kong B, *et al.* >23% High-efficiency tunnel oxide junction bifacial solar cell with electroplated Cu gridlines. *IEEE J Photovolt*. 2015; 5(1):82–6.
- [111] Longi Solar. Longi achieves 25.21% efficiency for TOPCon solar cell, 2021.
- [112] Pham DP, Lee S, Kim Y, and Yi J. Band-offset reduction for effective hole carrier collection in bifacial silicon heterojunction solar cells. *J Phys Chem Solids*. 2021;154:110059.
- [113] Schmiga C, Grubel B, Cimiotti G, *et al.* 23.8% efficient bifacial i-TOPCon silicon solar cells with <20 μ m wide Ni/Cu/Ag-plated contact fingers. In: *Metallization and Interconnection Workshop*, 2021, Genk, Belgium.
- [114] Schultz-Wittmann O, De Ceuster D, Turner A, *et al.* Fine line copper based metallization for high efficiency crystalline silicon solar cells. In: *Proceedings of the 27th European Photovoltaic Solar Energy Conference*. München: WIP; 2012, pp. 596–9.
- [115] Böscke TS, Kania D, Helbig A, *et al.* Bifacial n-type cells with >20% front-side efficiency for industrial production. *IEEE J Photovolt.* 2013;3 (2):674–7.
- [116] Tous L, Russell R, Cornagliotti E, *et al.* 22.4% Bifacial n-PERT cells with Ni/Ag co-plated contacts and Voc~ 691 mV. *Energy Proc.* 2017;124: 922–9.

- [117] Wang J, Xuan Y, Zheng L, Xu Y, and Yang L. Improvement of bifacial heterojunction silicon solar cells with light-trapping asymmetrical bifacial structures. *Sol Energy*. 2021;223:229–37.
- [118] Wu W, Zhang Z, Zheng F, Lin W, Liang Z, and Shen H. Efficiency enhancement of bifacial PERC solar cells with laser-doped selective emitter and double-screen-printed Al grid. *Prog Photovolt Res Appl.* 2018;26(9):752–60.
- [119] Yu B, Shi J, Li F, *et al.* Selective tunnel oxide passivated contact on the emitter of large-size n-type TOPCon bifacial solar cells. *J Alloys Compd.* 2021;870:159679.
- [120] Yu J, Bian J, Duan W, *et al.* Tungsten doped indium oxide film: ready for bifacial copper metallization of silicon heterojunction solar cell. *Sol Energy Mater Sol Cells.* 2016;144:359–63.
- [121] Rodríguez-Gallegos CD, Liu H, Gandhi O, *et al.* Global techno-economic performance of bifacial and tracking photovoltaic systems. *Joule.* 2020; 4(7):1514–41.
- [122] Panasonic Solar, Panasonic Solar, 2018.
- [123] Intersolar Europe: SolarWorld to Launch Glass-Glass Bifacial Modules, 2015.
- [124] Liang TS, Pravettoni M, Singh JP, and Khoo YS. Meeting the requirements of IEC TS 60904-1-2 for single light source bifacial photovoltaic characterisation: evaluation of different back panel materials. *Eng Res Express*. 2020;2(1):015048.
- [125] Richter A, Hermle M, and Glunz SW. Reassessment of the limiting efficiency for crystalline silicon solar cells. *IEEE J Photovolt.* 2013; 3(4):1184–91.
- [126] Ingenito A, Isabella O, and Zeman M. Nano-cones on micro-pyramids: modulated surface textures for maximal spectral response and high-efficiency solar cells. *Prog Photovolt Res Appl.* 2015;23(11):1649–59.
- [127] Ingenito A, Isabella O, and Zeman M. Experimental demonstration of 4n 2 classical absorption limit in nanotextured ultrathin solar cells with dielectric omnidirectional back reflector. *ACS Photonics*. 2014;1(3): 270–8.
- [128] Niewelt T, Richter A, Kho TC, *et al.* Taking monocrystalline silicon to the ultimate lifetime limit. *Sol Energy Mater Sol Cells.* 2018;185:252–9.
- [129] Steinhauser B, Niewelt T, Richter A, Eberle R, and Schubert MC. Extraordinarily high minority charge carrier lifetime observed in crystalline silicon. *Sol RRL*. 2021;5(11):2100605.
- [130] Fell A, Niewelt T, Steinhauser B, Heinz FD, Schubert MC, and Glunz SW. Radiative recombination in silicon photovoltaics: modeling the influence of charge carrier densities and photon recycling. *Sol Energy Mater Sol Cells*. 2021;230:111198.
- [131] Veith-Wolf BA, Schäfer S, Brendel R, and Schmidt J. Reassessment of intrinsic lifetime limit in n-type crystalline silicon and implication on maximum solar cell efficiency. *Sol Energy Mater Sol Cells*. 2018;186:194–9.

- [132] Black LE, Macdonald DH. On the quantification of Auger recombination in crystalline silicon. *Sol Energy Mater Sol Cells*. 2022 Jan;234(September 2021):111428.
- [133] Blinn JF. Models of light reflection for computer synthesized pictures. In: *Proceedings of the 4th Annual Conference on Computer Graphics and Interactive Techniques SIGGRAPH '77.* New York, NY: ACM Press; 1977, pp. 192–8.
- [134] Niewelt T, Steinhauser B, Richter A, *et al.* Reassessment of the intrinsic bulk recombination in crystalline silicon. *Sol Energy Mater Sol Cells*. 2022;235:111467.
- [135] Dréon J, Jeangros Q, Cattin J, *et al.* 23.5%-Efficient silicon heterojunction silicon solar cell using molybdenum oxide as hole-selective contact. *Nano Energy.* 2020;70:104495.
- [136] PVMD Group, TU Delft. Certified measurement at ISFH CalTeC, Calmark: 002243, device area = 3.915 cm², η = (23.83 \pm 0.29)%, 13.01.2022.
- [137] Bullock J, Wan Y, Hettick M, *et al.* Dopant-free partial rear contacts enabling 23% silicon solar cells. *Adv Energy Mater*. 2019;9:1803367.
- [138] Yang X, Xu H, Liu W, *et al.* Atomic layer deposition of vanadium oxide as hole-selective contact for crystalline silicon solar cells. *Adv Electron Mater.* 2020;6(8):2000467.
- [139] Mazzarella L, Alcañiz A, Procel P, *et al.* Strategy to mitigate the dipole interfacial states in (i)a-Si:H/MoOx passivating contacts solar cells. *Prog Photovolt Res Appl.* 2021;29(3):391–400.
- [140] Matsui T, Bivour M, Hermle M, and Sai H. Atomic-layer-deposited TiOx nanolayers function as efficient hole-selective passivating contacts in silicon solar cells. *ACS Appl Mater Interfaces*. 2020;12(44):49777–85.
- [141] Lin W, Boccard M, Zhong S, *et al.* Degradation mechanism and stability improvement of dopant-free ZnO/LiFx/Al electron nanocontacts in silicon heterojunction solar cells. *ACS Appl Nano Mater.* 2020;3(11): 11391–8.
- [142] Sailor MJ, Ginsburg EJ, Gorman CB, Kumar A, Grubbs RH, and Lewis NS. Thin films of n-Si/poly-(CH3)3Si-cyclooctatetraene: conducting-polymer solar cells and layered structures. *Science*. 1990;249(4973): 1146–9.
- [143] Gowrishankar V, Scully SR, McGehee MD, Wang Q, and Branz HM. Exciton splitting and carrier transport across the amorphous-silicon/polymer solar cell interface. *Appl Phys Lett.* 2006;89(25):252102.
- [144] Liu C-Y, Holman ZC, and Kortshagen UR. Hybrid solar cells from P3HT and silicon nanocrystals. *Nano Lett.* 2009;9(1):449–52.
- [145] Sun K, Zhang S, Li P, *et al.* Review on application of PEDOTs and PEDOT:PSS in energy conversion and storage devices. *J Mater Sci Mater Electron.* 2015;26(7):4438–62.
- [146] Groenendaal L, Zotti G, Aubert P-H, Waybright SM, Reynolds JR. Electrochemistry of poly(3,4-alkylenedioxythiophene) derivatives. *Adv Mater.* 2003;15(11):855–79.

- [147] Heywang G and Jonas F. Poly(alkylenedioxythiophene)s—new, very stable conducting polymers. *Adv Mater.* 1992;4(2):116–8.
- [148] Zielke D, Niehaves C, Lövenich W, Elschner A, Hörteis M, and Schmidt J. Organic-silicon solar cells exceeding 20% efficiency. *Energy Proc.* 2015;77:331–9.
- [149] Yun MH, Kim JW, Park SY, Kim DS, Walker B, Kim JY.High-efficiency, hybrid Si/C60 heterojunction solar cells. *J Mater Chem A*. 2016 Oct 25; 4(42):16410–7.
- [150] Ji W, Allen T, Yang X, Zeng G, De Wolf S, and Javey A. Polymeric electron-selective contact for crystalline silicon solar cells with an efficiency exceeding 19%. *ACS Energy Lett.* 2020;5(3):897–902.
- [151] Vos AD. Detailed balance limit of the efficiency of tandem solar cells. *J Phys Appl Phys.* 1980;13(5):839–46.
- [152] Brown AS and Green MA. Detailed balance limit for the series constrained two terminal tandem solar cell. *Phys E Low-Dimens Syst Nanostruct*. 2002;14(1–2):96–100.
- [153] Futscher MH and Ehrler B. Efficiency limit of perovskite/si tandem solar cells. *ACS Energy Lett.* 2016;1(4):863–8.
- [154] Steirer KX, Schulz P, Teeter G, *et al.* Defect tolerance in methylammonium lead triiodide perovskite. *ACS Energy Lett.* 2016;1(2):360–6.
- [155] De Wolf S, Holovsky J, Moon S-J, *et al.* Organometallic halide perovskites: sharp optical absorption edge and its relation to photovoltaic performance. *J Phys Chem Lett.* 2014;5(6):1035–9.
- [156] Jäger K, Korte L, Rech B, and Albrecht S. Numerical optical optimization of monolithic planar perovskite-silicon tandem solar cells with regular and inverted device architectures. *Opt Express*. 2017;25(12): A473.
- [157] Aydin E, Allen TG, De Bastiani M, *et al.* Interplay between temperature and bandgap energies on the outdoor performance of perovskite/silicon tandem solar cells. *Nat Energy.* 2020 Nov;5(11):851–9.
- [158] Unger EL, Kegelmann L, Suchan K, Sörell D, Korte L, and Albrecht S. Roadmap and roadblocks for the band gap tunability of metal halide perovskites. *J Mater Chem A*. 2017;5(23):11401–9.
- [159] Bush KA, Palmstrom AF, Yu ZJ, *et al.* 23.6%-efficient monolithic perovskite/silicon tandem solar cells with improved stability. *Nat Energy*. 2017;2(4):17009.
- [160] Sahli F, Werner J, Kamino BA, *et al.* Fully textured monolithic perovskite/ silicon tandem solar cells with 25.2% power conversion efficiency. *Nat Mater*. 2018;17(9):820–6.
- [161] Al-Ashouri A, Magomedov A, Roß M, *et al.* Conformal monolayer contacts with lossless interfaces for perovskite single junction and monolithic tandem solar cells. *Energy Environ Sci.* 2019;12(11):3356–69.
- [162] Al-Ashouri A, Köhnen E, Li B, *et al.* Monolithic perovskite/silicon tandem solar cell with >29% efficiency by enhanced hole extraction. *Science*. 2020;370(6522):1300–9.

- [163] Helmholtz-Zentrum Berlin für Materialien und Energie. World record again at HZB: Almost 30 % efficiency for next-generation tandem solar cells, 2021 [cited 2022 Feb 17]. Available from: https://www.helmholtz-berlin.de/pubbin/news_seite?nid=23248;sprache=en
- [164] NREL. Best Research-Cell Efficiency Chart. [cited 2022 Feb 28]. Available from: https://www.nrel.gov/pv/cell-efficiency.html
- [165] Jošt M, Lipovšek B, Glažar B, *et al.* Perovskite solar cells go outdoors: field testing and temperature effects on energy yield. *Adv Energy Mater*. 2020;10(25):2000454.
- [166] Messmer C, Schön J, Lohmüller S, et al. How to make PERC suitable for perovskite–silicon tandem solar cells: a simulation study. Prog Photovolt Res Appl. 2022;early view. [cited 2022 Jan 24]. Available from: https://onlinelibrary.wiley.com/doi/abs/10.1002/pip.3524
- [167] Mariotti S, Jäger K, Diederich M, et al. Monolithic perovskite/silicon tandem solar cells fabricated using industrial p-type polycrystalline silicon on oxide/passivated emitter and rear cell silicon bottom cell technology. Sol RRL. 2022;n/a:2101066.
- [168] Essig S, Allebé C, Remo T, *et al.* Raising the one-sun conversion efficiency of III–V/Si solar cells to 32.8% for two junctions and 35.9% for three junctions. *Nat Energy.* 2017;2(9):1–9.
- [169] Schygulla P, Müller R, Lackner D, *et al.* Two-terminal III–V//Si triple-junction solar cell with power conversion efficiency of 35.9 % atAM1.5g. *Prog Photovolt Res Appl.*; n/a(n/a) [cited2021 Nov 12]. Available from: https://onlinelibrary.wiley.com/doi/abs/10.1002/pip.3503
- [170] Vurgaftman I, Meyer JR, and Ram-Mohan LR. Band parameters for III–V compound semiconductors and their alloys. *J Appl Phys.* 2001;89(11): 5815–75.
- [171] B. Bolkhovityanov Y and P. Pchelyakov O. III–V Compounds-on-Si: heterostructure fabrication, *application and prospects*. Open Nanosci J. 2009 Oct 27 [cited 2022 Feb 28];3(1). Available from: https://benthamopen.com/ABSTRACT/TONANOJ-3-20
- [172] Grassman TJ, Brenner MR, Rajagopalan S, *et al.* Control and elimination of nucleation-related defects in GaP/Si(001) heteroepitaxy. *Appl Phys Lett.* 2009;94(23):232106.
- [173] Warren EL, Kibbler AE, France RM, Norman AG, Stradins P, and McMahon WE. Growth of antiphase-domain-free GaP on Si substrates by metalorganic chemical vapor deposition using an in situ AsH3 surface preparation. *Appl Phys Lett.* 2015;107(8):082109.
- [174] Grassman TJ, Chmielewski DJ, Carnevale SD, Carlin JA, and Ringel SA. GaAs0.75P0.25/Si dual-junction solar cells grown by MBE and MOCVD. *IEEE J Photovolt*. 2016;6(1):326–31.
- [175] Feifel M, Lackner D, Schön J, *et al.* Epitaxial GaInP/GaAs/Si triple-junction solar cell with 25.9%AM1.5g efficiency enabled by transparent metamorphic Al_xGa_{1-x}AsyP_{1-y} step-graded buffer structures. *Sol RRL*. 2021;5(5):2000763.

- [176] Veinberg-Vidal E, Vauche L, Medjoubi K, *et al.* Characterization of dual-junction III–V on Si tandem solar cells with 23.7% efficiency under low concentration. *Prog Photovolt Res Appl.* 2019;27(7):652–61.
- [177] Mizuno H, Makita K, and Matsubara K. Electrical and optical interconnection for mechanically stacked multi-junction solar cells mediated by metal nanoparticle arrays. *Appl Phys Lett.* 2012;101(19):191111.
- [178] Makita K, Mizuno H, Tayagaki T, *et al.* III–V//Si multijunction solar cells with 30% efficiency using smart stack technology with Pd nanoparticle array. *Prog Photovolt Res Appl.* 2020;28(1):16–24.
- [179] Victoria M, Haegel N, Peters IM, *et al.* Solar photovoltaics is ready to power a sustainable future. *Joule.* 2021;5(5):1041–56.
- [180] Ritchie H and Roser M. Renewable Energy | Our World in Data. Our World in Data. 2020 [cited 2022 Feb 22]. Available from: https://ourworldindata.org/renewable-energy
- [181] Sustainable Development Goals | United Nations Development Programme. United Nations Development Programme. [cited 2022 Feb 22]. Available from: https://www.undp.org/sustainable-development-goals
- [182] Global Wind Report 2021. Global Wind Energy Council. 2021 [cited 2022 Feb 22]. Available from: https://gwec.net/global-wind-report-2021/
- [183] Solar PV Renewables 2020 Analysis. IEA. [cited 2022 Feb 22]. Available from: https://www.iea.org/reports/renewables-2020/solar-pv
- [184] Utility scale solar reaches LCOE of \$0.028-\$0.041/kWh in the US, Lazard finds. *PV Magazine International*. [cited 2022 Feb 22]. Available from: https://www.pv-magazine.com/2021/11/05/utility-scale-solar-reaches-lcoe-of-0-028-0-041-kwh-in-the-us-lazard-finds/
- [185] Levelized Cost of Electricity: Renewables Clearly Superior to Conventional Power Plants Due to Rising CO2 Prices Fraunhofer ISE. Fraunhofer Institute for Solar Energy Systems ISE. [cited 2022 Feb 22]. Available from: https://www.ise.fraunhofer.de/en/press-media/press-releases/2021/levelized-cost-of-electricity-renewables-clearly-superior-to-conventional-power-plants-due-to-rising-co2-prices.html
- [186] Wade W. Power Plants Get More Expensive But Renewables Still Cheapest. Bloomberg.com. 2021 Dec 21 [cited 2022 Feb 22]; Available from: https://www.bloomberg.com/news/articles/2021-12-21/power-plants-get-more-expensive-but-renewables-still-cheapest
- [187] Vuichard P, Broughel A, Wüstenhagen R, Tabi A, and Knauf J. Keep it local and bird-friendly: exploring the social acceptance of wind energy in Switzerland, Estonia, and Ukraine. *Energy Res Soc Sci.* 2022;88: 102508.
- [188] Ritchie H and Roser M. Urbanization | Our World in Data. Our World Data. 2018 Jun 13 [cited 2022 Feb 22]; Available from: https://ourworldindata.org/urbanization
- [189] Calcabrini A, Muttillo M, Weegink R, Manganiello P, Zeman M, and Isabella O. A fully reconfigurable series-parallel photovoltaic module for higher energy yields in urban environments. *Renew Energy*. 2021;179:1–11.

- [190] Ziar H, Manganiello P, Isabella O, and Zeman M. Photovoltatronics: intelligent PV-based devices for energy and information applications. *Energy Environ Sci.* 2021;14(1):106–26.
- [191] Fraunhofer Institute for Solar Energy Systems, ISE. *Photovolt Report*. 2021;2021:50.
- [192] Solar continues to break installation records, on track for Terawatt scale by 2022 SolarPower Europe. SolarPower Europe. [cited 2022 Feb 22]. Available from: https://www.solarpowereurope.org/solar-continues-to-break-installation-records-on-track-for-terawatt-scale-by-2022/
- [193] Jinko Solar. JinkoSolar's High-efficiency N-Type Monocrystalline Silicon Solar Cell Sets Our New Record with Maximum Conversion Efficiency of 26.4%, 2022. https://www.jinkosolar.com/en/site/newsdetail/1827
- [194] World record back at HZB: Tandem solar cell achieves 32.5 percent efficiency. [cited 2023 Jan 05]. Available from: https://www.helmholtz-berlin.de/pubbin/news_seite?nid=24348&sprache=en&seitenid=1